# MECHANICAL IMPEDANCE CONTROL OF ROBOTIC MANIPULATORS IN CARTESIAN COORDINATES

by

Daniel Backer Grunberg

Submitted to the

DEPARTMENT OF ELECTRICAL ENGINEERING AND COMPUTER SCIENCE

in partial fulfillment of the requirements

FOR THE DEGREES OF

BACHELOR OF SCIENCE

and

MASTER OF SCIENCE

at the

MASSACHUSETTS INSTITUTE OF TECHNOLOGY

June, 1983



Signature of Auth .....
Department of Electrical Engineering and Computer Science,
May 16, 1983

Certified by.....Michael Athans.....
Thesis Supervisor (Academic)

Certified by. .....H. Austin Spang III.....
rvisor (Cooperating Company)

Accepted by.....Arthur C. Smith.....
Chairman, Departmental Committee on Graduate Students

# MECHANICAL IMPEDANCE CONTROL OF ROBOTIC MANIPULATORS IN CARTESIAN COORDINATES

by

Daniel Backer Grunberg

Submitted to the Department of Electrical Engineering and Computer Science on May 6, 1983 in partial fulfillment of the requirements for the Degrees of Master of Science and Bachelor of Science in Electrical Engineering and Computer Science.

## ABSTRACT

The design of a linear controller for the implementation of impedance control is considered. Impedance control refers to the specification of the mechanical impedance of the manipulator seen from the external environment. The stability of the complete system is analyzed and a method for reducing the effect of Jacobian matrices with large condition numbers on stability test conservativeness is derived. An actual implementation on the Rhino XR-1 robot was built and the usefulness of impedance control for the performance of certain tasks was demonstrated.

Thesis Supervisor: Dr. Michael Athans
Title: Professor of Systems Science and Engineering

Company Supervisor: Dr. H. Austin Spang III
Title: Adjunct Professor/G.E. Supervisor

ACKNOWLEDGEMENTS

I would like to thank Professor Michael Athans and Dr. H. Austin Spang III for their guidance and suggestions during the course of this project, as well as for their reading of the drafts of the thesis.

The experimental part of this thesis was conducted at the Control Technology Branch of Corporate Research & Development, General Electric Co., Schenectady, New York as part of the MIT Department of Electrical Engineering and Computer Science Cooperative Program (VI-A) and I am grateful to have had the opportunity to participate in the co-op program. For their support and advice while I was in Schenectady, I would like to also thank Dr. John Cassidy, as well as Anna Grooms, Bob Smith, Ed Slate, Ken Haefner, and Walt Whipple III.

Special thanks are also deserved by Mike Alter and Jack Suitto of the Materials and Processes Laboratory, G.E. for the superb equipment they designed and built.

In addition I would like to thank John Iler for taking time from his important activities for his thoughts on a draft of my thesis.

To my Family

TABLE OF CONTENTS

LIST OF FIGURES

## LIST OF TABLES



## LIST OF PHOTOGRAPHS

# 1. INTRODUCTION

## 1.1 WHAT IS FORCE CONTROL?

Force control, as used in robotics, refers to a manipulator system in which the interaction force between the manipulator and its environment can affect the manipulator's position. This is in contrast to a typical position-controlled manipulator, where position commands are executed without regard to the force exerted on objects being handled. In a force control system, both force and position information are fed back, as shown in Fig. 1-1.

Force control can take many different forms. One type is termed Hybrid control (Mason 1981) where different axes are specified as either pure force control or pure position control. Pure force control means that a force, e.g. 4.8 oz, is specified in a given direction, and the controller attempts to maintain that level of force.

Another form of force control which is in a sense more general than Hybrid control is impedance control, where the mechanical impedance of the manipulator arm seen from the external environment is specified arbitrarily (Hogan 1982). A simple example of this would be specifying the spring constant of the manipulator about any desired set point. The system would then look as if it were built out of springs; the two-dimensional case is shown in Fig. 1-2. Commanded positions, $\underline{r}$, would serve to move the "frame", with the actual position of the

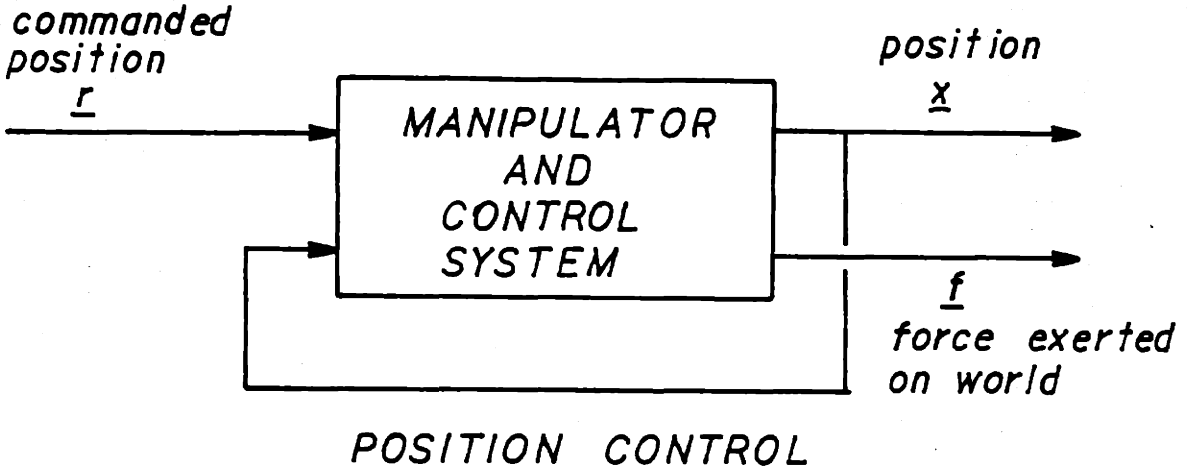


POSITION CONTROL

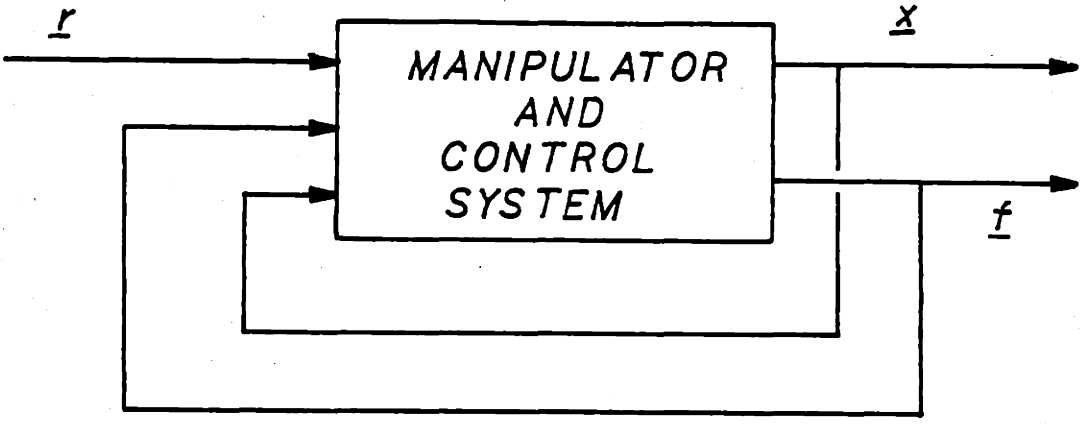


FORCE CONTROL

FIGURE 1-1: COMPARISON OF POSITION CONTROL AND FORCE CONTROL

end-effector, $\underline{x}$, depending on the environment and the interaction force, $\underline{f}$.

## 1.2 BENEFITS OF FORCE CONTROL

Some of the advantages of force control are immediately apparent. Any robotics application dealing with fragile objects could benefit from force control, as well as any where obstacles (possibly living) may be present but whose location is unknown.

Another application for force control is one involving uncertainty. Consider the problem of trying to write on a table whose vertical position is known to within two inches. A human has no difficulty with this maneuver as force information is utilized unconsciously. With force control, a robot can also perform this task without writing uselessly in the air or destroying the pen. Other examples where force control obviates the need for precise positional information include closing a door, turning a crank, and fitting a bolt into a hole of uncertain position. In closing a door or turning a crank, a purely positional controller would need to know the exact radius of the path required.

## 1.3 IMPEDANCE CONTROL

Impedance control, as mentioned above, is a type of force control which is fairly general. It consists of specifying the mechanical impedance (mass, viscocity, and spring constant) of the end-effector. The actual-concept of impedance control was

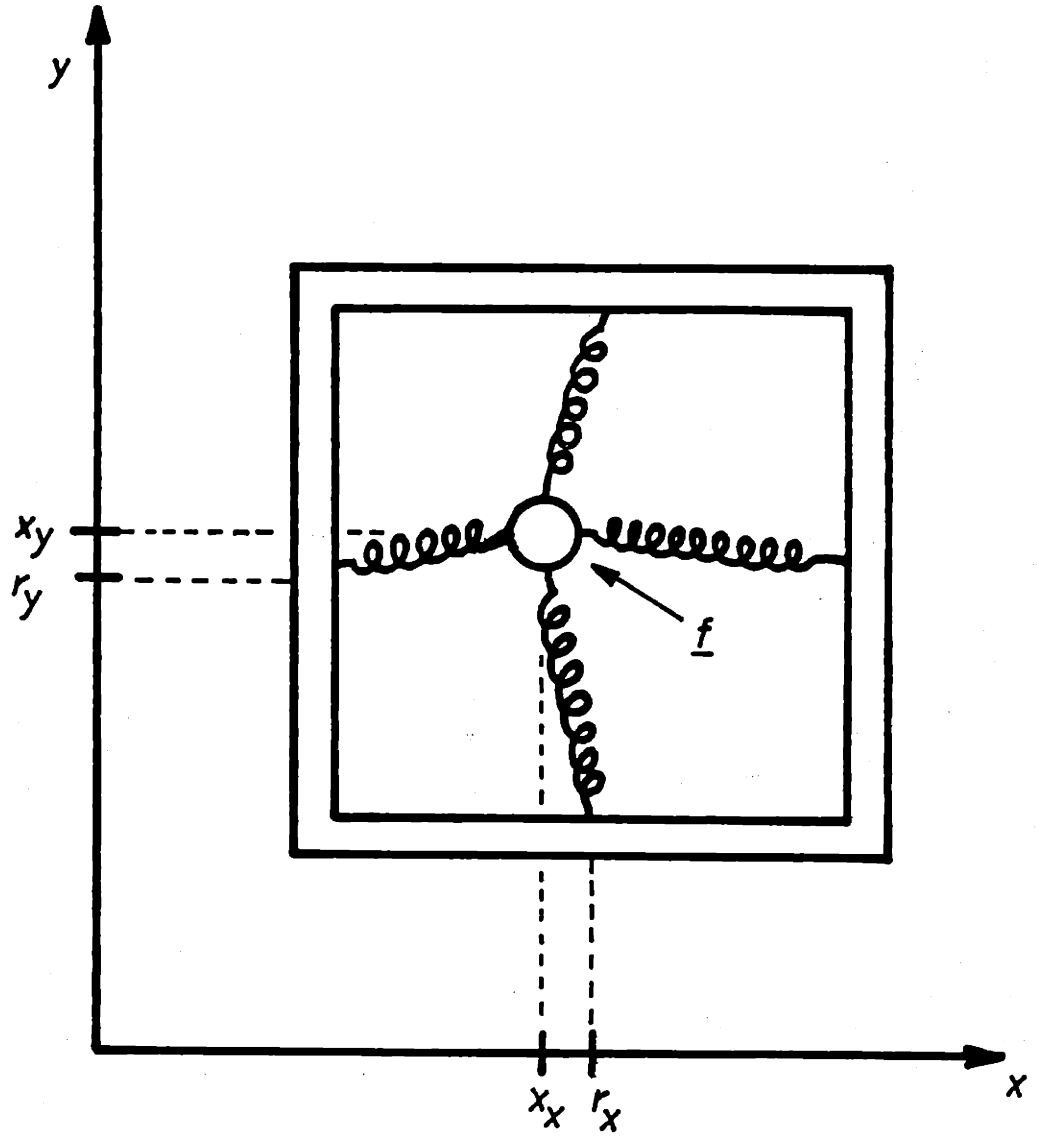


FIGURE 1-2: SIMPLE IMPEDANCE CONTROL (STIFFNESS)

described by Hogan and Cotter (1982).

An impedance controlled manipulator can act like a hybrid control system, with the proper choice of parameters. If a very high stiffness is commanded, a purely positional controller is approximated. If some axes are specified as very low stiffness, they are virtually pure force controlled as the rate of change of force with position will then be very small. Fig. 1-3 shows pictorially a system with position control in the x-axis and pure force control (virtually) in the y-axis.

Because of the generality of impedance control and its relative simplicity of specification (i.e. Mass-Damping-Stiffness), it will considered further. This thesis will be concerned with the design of an impedance controlled manipulator system. Additional justification will not be given for the actual use of impedance control nor for the selection of desired parameters.

## 1.4 PRESENTATION of PROBLEM

Here then is the impedance control problem that will be examined in this thesis:

Design a controller to implement impedance control for a robotic manipulator. The design should be done keeping in mind that it will actually be implemented on a small research robot, the Rhino XR-1 (see section 4.2). Thus it should be practical and make reasonable approximations and assumptions. Hopefully, the structure of the controller will not depend on the exact

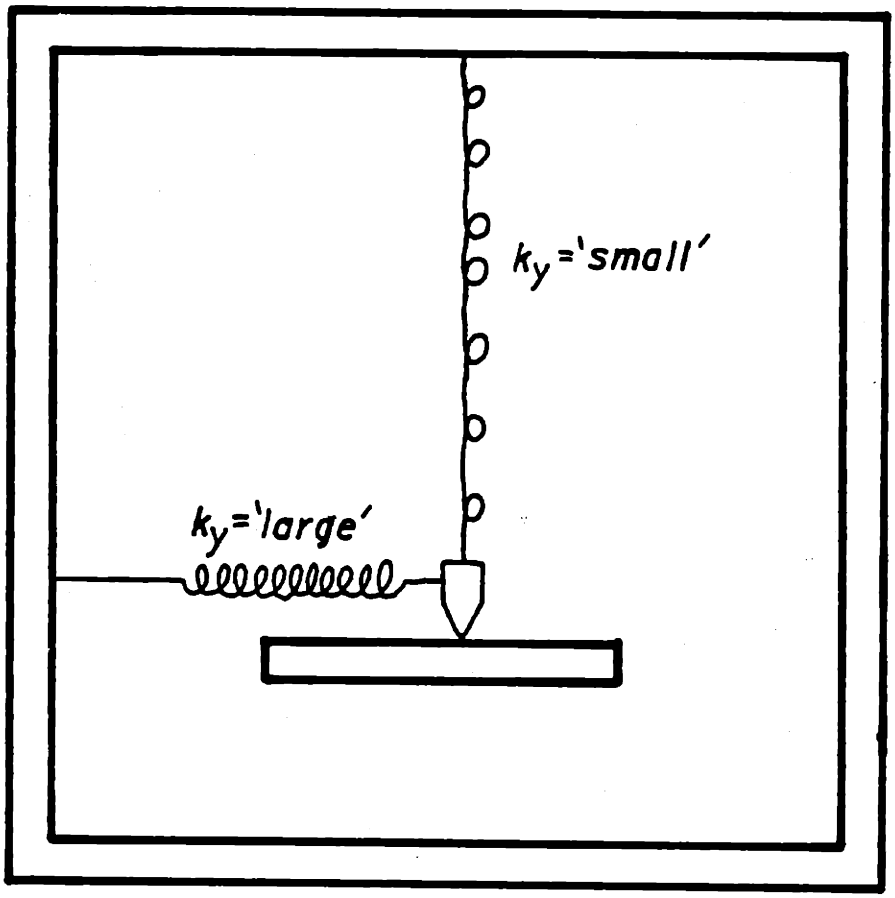


FIGURE 1-3: IMPEDANCE CONTROL SIMULATING HYBRID CONTROL

robot parameters.

## 1.5 CONTRIBUTIONS

There are two parts to this thesis: analytical and experimental. The contribution of the analytical part consists of presenting a structure for a controller and demonstrating its feasibility. It is shown that the structure presented will function correctly for proper choice of parameter values. Some problems due to both the nature of the impedance control problem and the coordinate transformations involved are indicated, as well as a possible method for partially overcoming them.

The experimental part of this thesis consists of the actual demonstration of an impedance control system on a real robot. Due to real-time computation limitations and to simplify the implementation, only a controlled-stiffness manipulator (i.e. mass and damping in impedance specification are zero) was built, but it still serves to demonstrate the usefulness of impedance control.

## 1.6 NOTATION

| | |
|---|---|
| $\underline{A}^H$ | complex conjugate transpose of the matrix $\underline{A}$. |
| $\underline{A}^T$ | transpose of the matrix $\underline{A}$. |
| det $\underline{A}$ | determinant of the matrix $\underline{A}$. |
| $\lambda_i(\underline{A})$ | $i^{th}$ eigenvalue of $\underline{A}$, $\lambda_n > \lambda_{n-1} > \ldots > \lambda_1$ |
| $\sigma_i(\underline{A})$ | $i^{th}$ singular value of $\underline{A}$ = $\lambda_i^{1/2}(\underline{A}^H \underline{A})$. |
| $\underline{I}$ | identity matrix. |
| $\underline{A}^{-1}$ | inverse of the matrix $\underline{A}$. |
| $\|x\|$ | magnitude of the scalar x. |
| $\|\|\underline{x}\|\|_2$ | euclidean norm of the vector $\underline{x}$. |
| $\|\|\underline{A}\|\|$ | maximum singular value of the matrix $\underline{A}$. |
| $\underline{A} \geq \underline{0}$ | $\underline{A}$ is positive semidefinite. |
| $\underline{A} > \underline{0}$ | $\underline{A}$ is positive definite. |

# 2. PRELIMINARY ANALYSIS

## 2.1 INTRODUCTION

The purpose of this chapter is to provide a preliminary view of several facets of the impedance control problem. The basics will be provided here as background for the linear controller development of chapter 3.

Section 2.2 provides a historical perspective of force control results previously published, related to both hybrid methods as well as impedance control.

Section 2.3, 2.4, and 2.5 give modeling details for the environment, the manipulator, and the reference model, respectively.

## 2.2 HISTORICAL OVERVIEW

### 2.2.1 Hybrid Control

Hybrid control, as described by Mason (1981), consists of partitioning the degrees of freedom of a manipulator into force-controlled axes and position-controlled axes. This is done so that the motion of the manipulator is compatible with the so-called natural constraints of the environment. For movements along a surface, that surface represents the natural constraints imposed by the environment. Position control into the surface is meaningless as is pure force control tangent to the surface. No forces can be exerted by an object (the manipulator) in free

space.

Hybrid control is in a sense open-loop because while the measured force is used on the force control axes, the form of the environment is assumed known—this information is in fact used in deciding how to partition the axes of the manipulator. No measured information regarding the shape of the environment is utilized by the controller.

Mason discusses such a hybrid mechanism for force control; no dynamical control issues are addressed. He deals mainly with the mathematical framework for conceptual development of hybrid control from an artificial intelligence viewpoint. He deals only with ideal (perfectly inelastic) surfaces and mentions that in going from one surface to another, one uses "guarded moves", in which the manipulator moves slowly until a force is sensed telling the controller that the surface has been reached. He does not discuss the implementation of these "guarded moves".

### 2.2.2 Impedance Control

Impedance control describes a system in which the mechanical impedance of the manipulator is specified arbitrarily. This general approach was defined by Hogan and Cotter (1982), and consists of defining a stiffness, viscous damping, and inertia desired for the end-effector as seen from the environment. In general, these can be nonlinear tensor quantities. In the linear case, to be considered in this thesis, the arm looks like a mass-spring-dashpot system with

adjustable parameters. Hogan and Cotter (1982) proposes an implementation of impedance control using a nonlinear pole-placement algorithm in which the manipulator dynamics are forced to look like the desired differential equation. This implementation requires an exact nonlinear model of the manipulator in order to function properly.

Specialized cases of the more general impedance control concept are the generalized spring and the generalized damper (Mason 1981).

A demonstration of the generalized spring is given by Andrews (1981), in which the force applied by the manipulator is proportional to the distance from some desired set point. Thus, it acts as a controlled-stiffness manipulator. Andrews' manipulator could turn a crank without exact knowledge of its radius. The design of the controller was done under quasi-static assumptions using motor currents to estimate forces, rather than external force sensors.

Another demonstration of the generalized spring is given by Salisbury (1980). This design uses feedback of measured forces, the control being done without analysis of stability of the whole system. The implementation includes rotational stiffness about three axes, as well as positional stiffness in 3-dimensions. He demonstrated his approach by an assembly problem involving the insertion of a stem of hexagonal cross-section into a matching hole.

Whitney (1977) presents a generalized damper in which the

velocity of the manipulator's end-effector is proportional to the external force applied. This is a special case of impedance control with zero stiffness and zero mass. His implementation assumes velocity-controlled servos and he gives stability conditions for the system based on both the desired manipulator impedance and the encountered environmental impedance. He worked with a decoupled manipulator without coordinate transformations.

The generalized damper is useful in certain types of assembly operations where a constant pressure on a non-moving object does not need to be applied. If this is not the case, stiffness is needed and the generalized damper will not suffice.

## 2.3 MODELING THE ENVIRONMENT

This section will present a model of the environment suitable for the purpose of the impedance control design of Chapter 3.

If the manipulator is in contact with an object in the environment, we can represent the force of interaction as being proportional to the displacement of the manipulator end-effector. Thus, we model it as a spring:

$$\underline{f}_K = \underline{K}_E (\underline{x} - \underline{d}) \qquad (2\text{-}1)$$

where $\underline{K}_E$ is a matrix representing the environmental spring constant.

$\underline{x}$ is the manipulator end-effector postion vector.

$\underline{d}$ is the offset induced by the object, since the object is not always at location $\underline{x} = \underline{0}$.

In addition to the proportional force due to deformation of the environment, there is a component due to accelerating any mass held in the gripper:

$$\underline{f}_m = m_E \ddot{\underline{x}} = \underline{M}_E \ddot{\underline{x}} \qquad (2\text{-}2)$$

where $\underline{M}_E = m_E \underline{I}$ = mass held in the gripper

$\ddot{\underline{x}}$ = acceleration vector of end-effector.

Combining $\underline{f}_K$ and $\underline{f}_M$, we obtain the block diagram of Fig. 2-1.

Note that in free space, $\underline{K}_E = 0$ and against a hard surface the norm of $\underline{K}_E$ is very large. Practically $\underline{K}_E$ is limited by the actual stiffness of the manipulator itself; pressing against a hard surface will cause bending in the manipulator's members.

Technically speaking, the above representation of the interaction force is inaccurate because that force is not shown affecting the manipulator dynamics. To be more accurate, the interaction force would feed into the manipulator model as a torque on the links of the manipulator. However, for small interaction forces, the representation of Fig. 2-1 is sufficient. The whole reason for using impedance control is to control the interaction forces and we do not want the forces so large that they alter the dynamics of the manipulator significantly; this would indicate straining of the motors, pulleys, etc.

From physical arguments of passivity, we know that

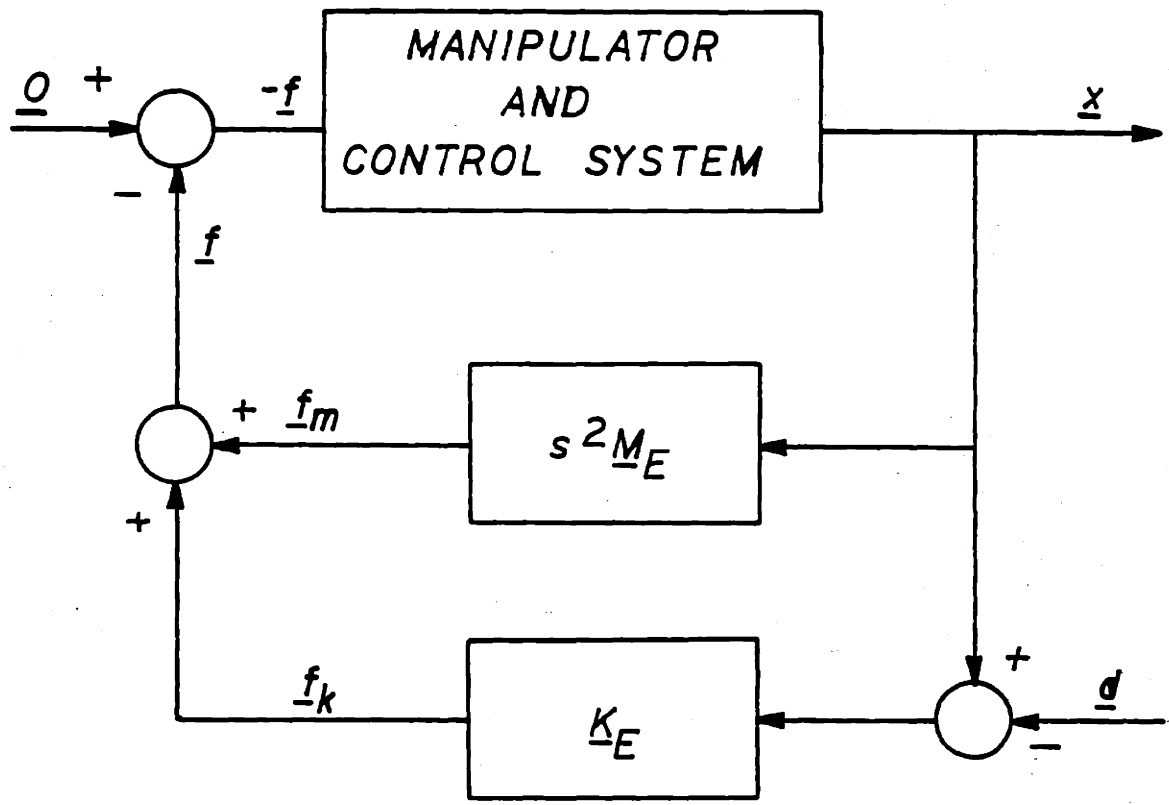


FIGURE 2-1: MODELING THE ENVIRONMENT

conditions on $\underline{K}_E$, $\underline{M}_E$ are

$$\underline{K}_E \geq 0 \quad (\det \underline{K}_E = 0 \text{ if against a smooth surface}),$$

$$\underline{M}_E = m_E \underline{I} \geq \underline{0}.$$

## 2.4 MODELING THE MANIPULATOR

### 2.4.1 Statics

In robotics it is frequently the case that the coordinate system most useful to describe the position of the manipulator's joints is not the most useful to describe points in the robot's workspace. The former system is termed joint coordinates while the latter task coordinates. Task coordinates are usually cartesian or cylindrical coordinates; they are chosen so as to make task specifications easy.

Let $\underline{\theta} = [\theta_1 \ \theta_2 \ \ldots \theta_n]^T$ be the n-vector of joint coordinates, where $\theta_i$ represents the position of joint i. Note that $\theta_i$ may not be in degrees ( e.g. a translational joint). Let $\underline{x} = [x_1 \ x_2 \ \ldots \ x_m]^T$ be the m-vector of task coordinates representing the position of the end-effector.

If $n<m$, we have a manipulator which cannot move about in our desired task-space. Either m must be reduced or a robot with more degrees of freedom must be considered. If $n>m$, then we have a redundant manipulator, or one in which we have extra degrees of freedom that must be specified. For a treatment of this case involving removing the redundancy, see Hewit and Padovan (1978).

The case m=n=3 will be considered here. Then there is a one-to-one mapping between joint positions and end-effector positions (barring redundancies in the joints such as two rotational joints with equivalent centers).

Let $\underline{x} = T(\underline{\theta})$ be the nonlinear transformation between coordinate frames. In general, $T(\underline{\theta})$ is obtainable, while $\underline{\theta} = \underline{T}^{-1}(\underline{x})$ rarely is in closed form. Any useful control algorithm should avoid the necessity of computing $\underline{T}^{-1}(\underline{x})$ directly. Now, we have

$$\underline{x} = [T_1(\underline{\theta})\ T_2(\underline{\theta})\ T_3(\underline{\theta})\ \ldots\ T_m(\underline{\theta})]^T \qquad (2\text{-}3)$$

Define $\underline{J} = [DT]$ as the Jacobian matrix of $\underline{T}(\underline{\theta})$. The mxn Jacobian matrix is defined as follows:

$$\underline{J} \triangleq [DT] \triangleq \begin{bmatrix} \frac{\partial T_1(\underline{\theta})}{\partial \theta_1} & \frac{\partial T_1(\underline{\theta})}{\partial \theta_2} & \frac{\partial T_1(\underline{\theta})}{\partial \theta_n} \\ \frac{\partial T_2(\underline{\theta})}{\partial \theta_1} & \frac{\partial T_2(\underline{\theta})}{\partial \theta_2} & \vdots \\ \frac{\partial T_m(\underline{\theta})}{\partial \theta_1} & \cdots & \frac{\partial T_m(\underline{\theta})}{\partial \theta_n} \end{bmatrix} \qquad (2\text{-}4)$$

Thus we can write

$$d\underline{x} = \underline{J} d\underline{\theta} \tag{2-5}$$

$$\Delta\underline{x} \cong \underline{J}\,\Delta\underline{\theta} \tag{2-6}$$

$$\text{and } \dot{\underline{x}} = \underline{J}\,\dot{\underline{\theta}} \text{ or } \dot{\underline{\theta}} = \underline{J}^{-1}\dot{\underline{x}} \tag{2-7}$$

for infinitesmal $d\underline{x}$, $d\underline{\theta}$ or small $\Delta\underline{x}, \Delta\underline{\theta}$ (2-7) allows us to decide what direction to move in joint coordinates, given a direction in task coordinates. This is used in a robot-control technique call "Resolved-motion-rate control" (Hewit and Burdess 1980). It is a linearization of the nonlinear coordinate transformations used with small incremental variables.

Consider the simple two-link manipulator shown in Fig. 2-2. Note that the standard way of defining angles for manipulators is for $\phi_2$ to represent the angle of deflection in the center joint; however, the Rhino XR-1, to be used for demonstration purposes, is more easily described as in Fig. 2-2.

From simple trigonometry, we have

$$\underline{x} = \begin{bmatrix} x \\ y \end{bmatrix} = T(\underline{\theta}) = d\begin{bmatrix} \sin(\phi_1) + \sin(\phi_2) \\ \cos(\phi_1) + \cos(\phi_2) \end{bmatrix} \tag{2-8}$$

While equal length links were assumed here, unequal length arms can be treated in a similar manner.

Taking derivatives,

$$\underline{J} = d\begin{bmatrix} \cos(\phi_1) & \cos(\phi_2) \\ -\sin(\phi_1) & -\sin(\phi_2) \end{bmatrix} \tag{2-9}$$

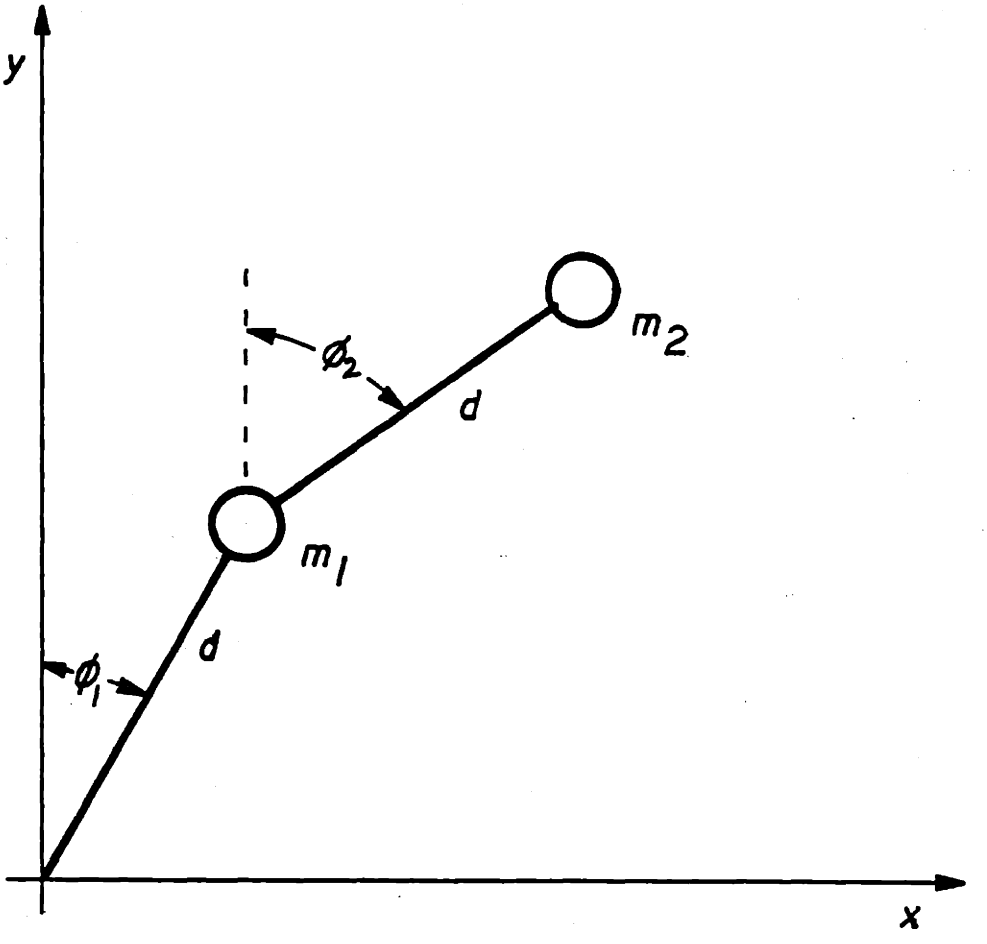


FIGURE 2-2: SIMPLE TWO-LINK MANIPULATOR

Note that $\det \underline{J} = -d[\sin(\phi_2)\cos(\phi_1) - \cos(\phi_2)\sin(\phi_1)]$

$$= d\sin(\phi_1 - \phi_2) \qquad (2\text{-}10)$$

Therefore $\det \underline{J} = 0$ occurs only if $\phi_2 = \phi_1$ or $\phi_2 = \phi_1 + 180°$.

The Jacobian is singular when the manipulator is either at the origin or on a circle of radius 2d.

## 2.4.2 Dynamics

This section will present a short deviation of the dynamical equations for a two-link manipulator as shown in Fig. 2-2. For a more complete and general derivation (n-link manipulator) see Paul (1981), Chapter 6. Consider the manipulator modeled in Fig. 2-2, with masses $m_1$ and $m_2$.

The dynamical equations for a mechanical system can be written

$$F_i = \frac{d}{dt}\frac{\partial L}{\partial \dot{q}_i} - \frac{\partial L}{\partial q_i} \qquad i = 1, 2, \ldots, n. \tag{2-11}$$

where $q_i$ = generalized coordinate (distance or angle)

$\dot{q}_i$ = generalized velocity

$F_i$ = corresponding force or torque

$L$ = the Lagrangian, defined as the differnce between the the kinetic and potential energy of the system.

By writing the kinetic energy of each mass—$m_2$ is easier done in cartesian coordinates—and potential energy, the Lagrangian can be found. The resulting equations of motion are:

$$\tau_1 = D_{11}\ddot{\phi}_1 + D_{12}\ddot{\phi}_2 + D_{111}\dot{\phi}_1^2 + D_{122}\dot{\phi}_2^2 + D_{112}\dot{\phi}_1\dot{\phi}_2 + D_{121}\dot{\phi}_2\dot{\phi}_1 + D_1 \tag{2-12}$$

$$\tau_2 = D_{12}\ddot{\phi}_1 + D_{22}\ddot{\phi}_2 + D_{211}\dot{\phi}_1^2 + D_{222}\dot{\phi}_2^2 + D_{212}\dot{\phi}_1\dot{\phi}_2 + D_{221}\dot{\phi}_2\dot{\phi}_1 + D_2 \tag{2-13}$$

where

$\tau_i$ = torque at $i^{th}$ joint

$$D_{11} = d^2[m_1 + 2m_2 + 2m_2\cos\phi_2] \tag{2-14}$$

$$D_{12} = d^2 m_2[1 + \cos\phi_2] \tag{2-15}$$

$$D_{22} = d^2 m_2 \tag{2-16}$$

(2-14), (2-15), (2-16): coupling inertias relating the accelaration at one joint to the torque at another (or the same one).

$$D_{122} = -m_2 d_2 \sin\phi_2 \qquad (2\text{-}17)$$

$$D_{211} = -m_2 d_2 \sin\phi_2 \qquad (2\text{-}18)$$

centripetal acceleration coefficients

$$D_{222} = 0 \qquad (2\text{-}19)$$

$$D_{112} = D_{121} = -m_2 d_2 \sin\phi_2 \qquad (2\text{-}20)$$

$$D_{212} = D_{221} = -m_2 d_2 \sin\phi_2 \qquad (2\text{-}21)$$

coriolis coefficients

$$D_1 = -(m_1 + m_2) g d \sin\phi_1 + m_2 g d \sin(\phi_1 + \phi_2) \qquad (2\text{-}22)$$

$$D_2 = m_2 g d \sin(\phi_1 + \phi_2) \qquad (2\text{-}23)$$

gravity terms

where $g$ = acceleration due to gravity

In vector form, we can write

$$\underline{\tau} = \underline{D}(\underline{\theta})\,\ddot{\underline{\theta}} + \underline{C}(\underline{\theta}, \dot{\underline{\theta}}) + \underline{G}(\underline{\theta}). \qquad (2\text{-}24)$$

$$\underline{D}(\underline{\theta}) = \begin{bmatrix} D_{11} & D_{12} \\ D_{12} & D_{22} \end{bmatrix}$$

## 2.4.3 Manipulator System Equations

In order to extract usable information from the above full nonlinear dynamic equations, some engineering approximations will have to be made. Furthermore, terms ignored above (e.g. friction) may well be larger than the second order effects which will be removed here.

If speeds are below some threshold, we can ignore the coriolis and centripetal terms. This threshold could be increased through the use of velocity feedback, if necessary. When linearized about an operating point, the nonlinear terms are seen as viscous damping terms. The gravity terms will be treated as disturbances and ignored here. Inverting the inertial terms,

$$\underline{\tau} = \underline{D}(\underline{\theta})\,\ddot{\underline{\theta}} \qquad (2\text{-}25)$$

we obtain $\ddot{\underline{\theta}} = \underline{P}(\underline{\theta})\,\underline{\tau}$, where $\underline{P}(\underline{\theta}) = \underline{D}^{-1}(\underline{\theta})$.

It will be assumed that DC electric motors are used to drive the joints with a voltage source drive system for the motors. Our system now looks like Fig. 2-3.

Here

$\underline{u}$ = input voltage to motor

$\underline{\tau}$ = torque applied to motor shaft

$\underline{K}_T$ = motor gain [torque/amps]

$\underline{K}_V$ = motor back EMF [volts/rad/sec]

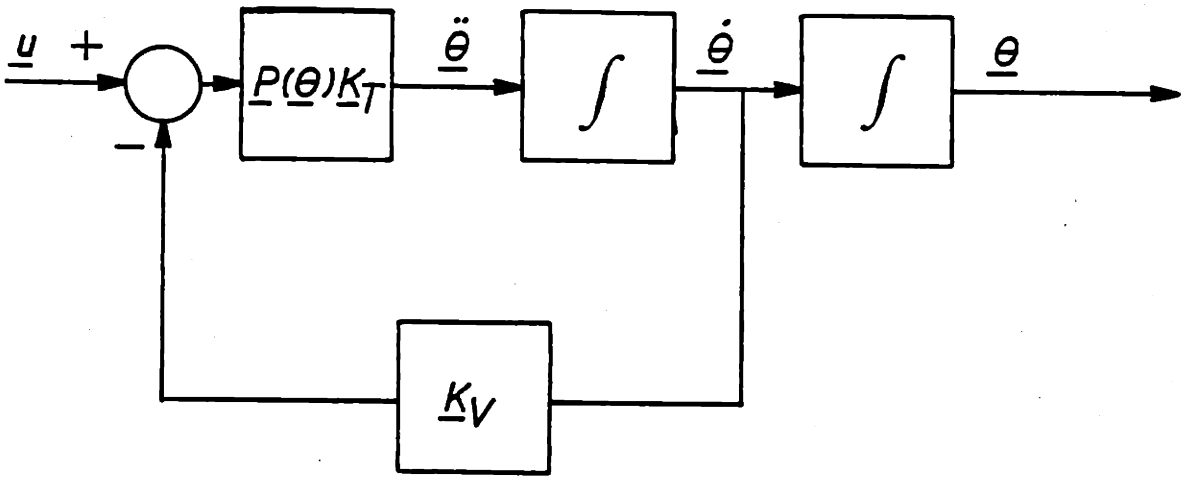


FIGURE 2-3: MOTORS AND MANIPULATOR SYSTEM

The system can be placed in state equation form as

$$\begin{bmatrix} \dot{\underline{\theta}} \\ \ddot{\underline{\theta}} \end{bmatrix} = \begin{bmatrix} \underline{0} & \underline{I} \\ \underline{0} & -P(\underline{\theta})\,\underline{K}_T\underline{K}_V \end{bmatrix} \begin{bmatrix} \underline{\theta} \\ \dot{\underline{\theta}} \end{bmatrix} + \begin{bmatrix} 0 \\ \underline{P}(\underline{\theta})\,\underline{K}_T \end{bmatrix} \underline{u} \qquad (2\text{-}26)$$

or $\dot{\underline{z}} = \underline{A}(\underline{\theta})\underline{z} + \underline{B}(\underline{\theta})\underline{u}$. (2-27)

From Fig. 2-3, we can see that the loop transmission of the motor loop is $(1/s)\underline{P}(\underline{\theta})\underline{K}_T\underline{K}_V$. Therefore, if

$$\sigma_{min}\left[\frac{1}{j\omega}\underline{P}(\underline{\theta})\underline{K}_T\underline{K}_V\right] >> 1 \quad \text{or} \quad \sigma_{min}[\underline{P}(\underline{\theta})\underline{K}_T\underline{K}_V] >> \omega \qquad (2\text{-}28)$$

we then have a velocity control with no coupling between the joints. For low frequencies the coupling is magnificent. The larger $\underline{K}_V$, the higher the frequency at which coupling becomes important. Fig 2-4 shows the frequency domain model in general and at low frequencies.

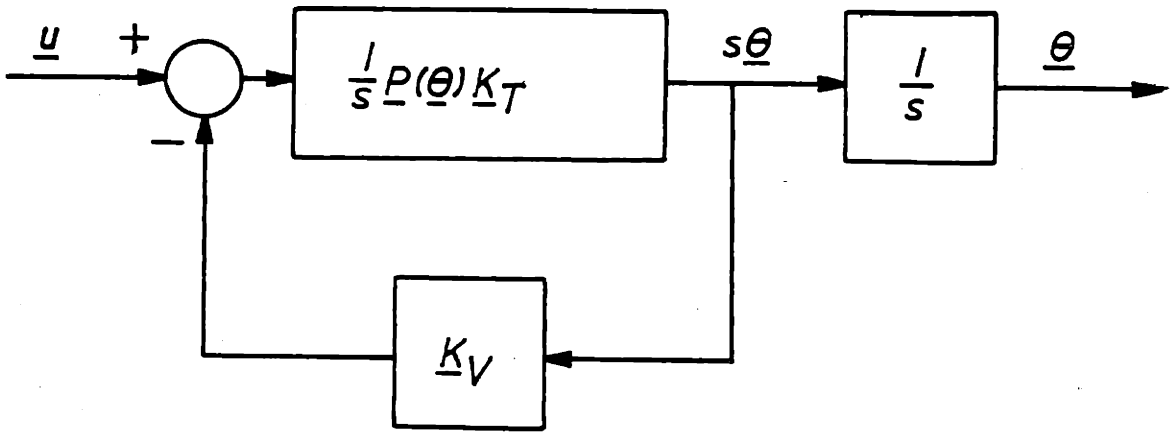


IN GENERAL

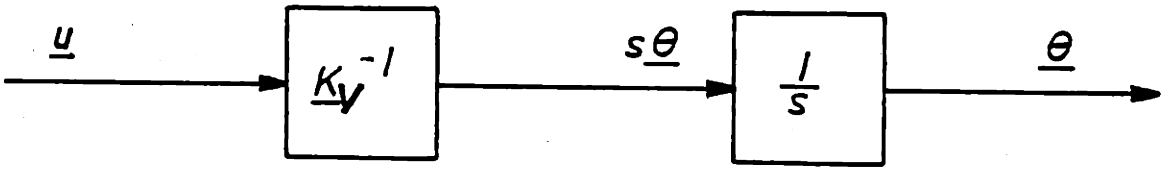


AT LOW FREQUENCIES

FIGURE 2-4: FREQUENCY DOMAIN MANIPULATOR MODEL

## 2.5 REFERENCE MODEL

Later on an explicit refernce model will be needed, it will be presented her first. Impedance control requires that the model have a dynamic equation:

$$\underline{M}\ddot{\underline{x}} = \underline{K}(\underline{r}-\underline{x}) - \underline{B}\dot{\underline{x}} + \underline{f} \qquad (2\text{-}29)$$

where $\underline{M}$, $\underline{K}$, $\underline{B}>\underline{0}$.

$\underline{M}=m\underline{I}$ $(m>0)$ for all physical masses. This equation results in Fig 2-5.. This can be implemented as in Fig. 2-6..

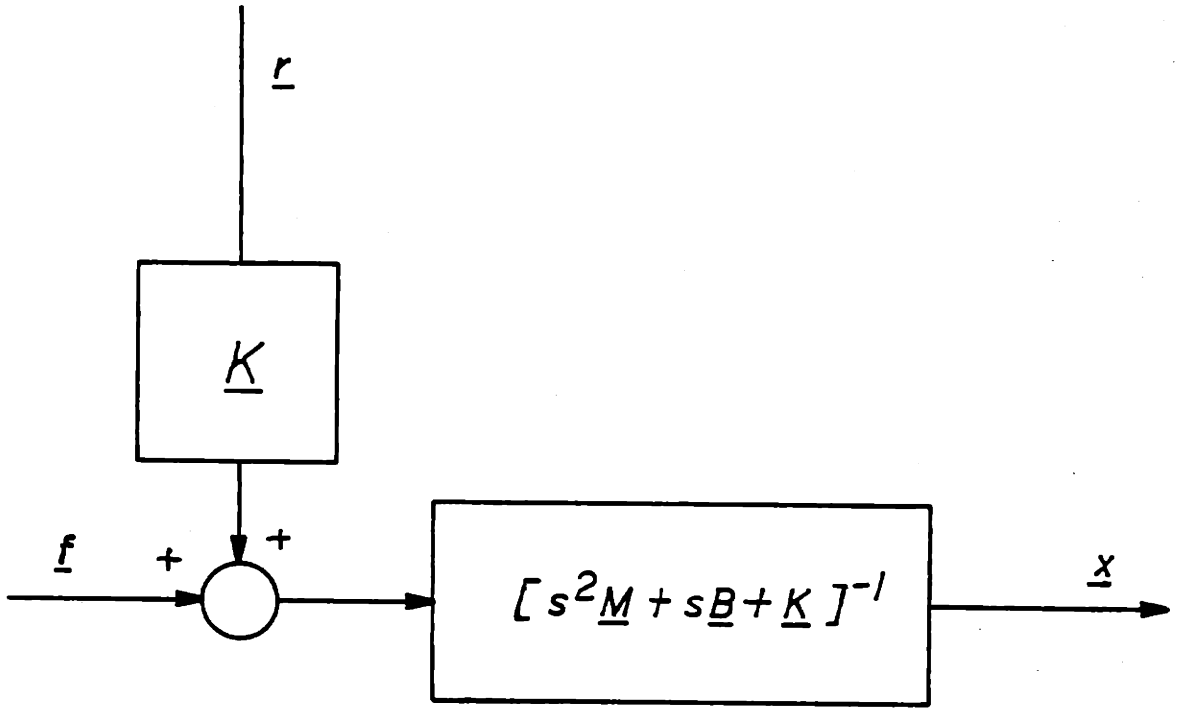


FIGURE 2-5: REFERENCE MODEL

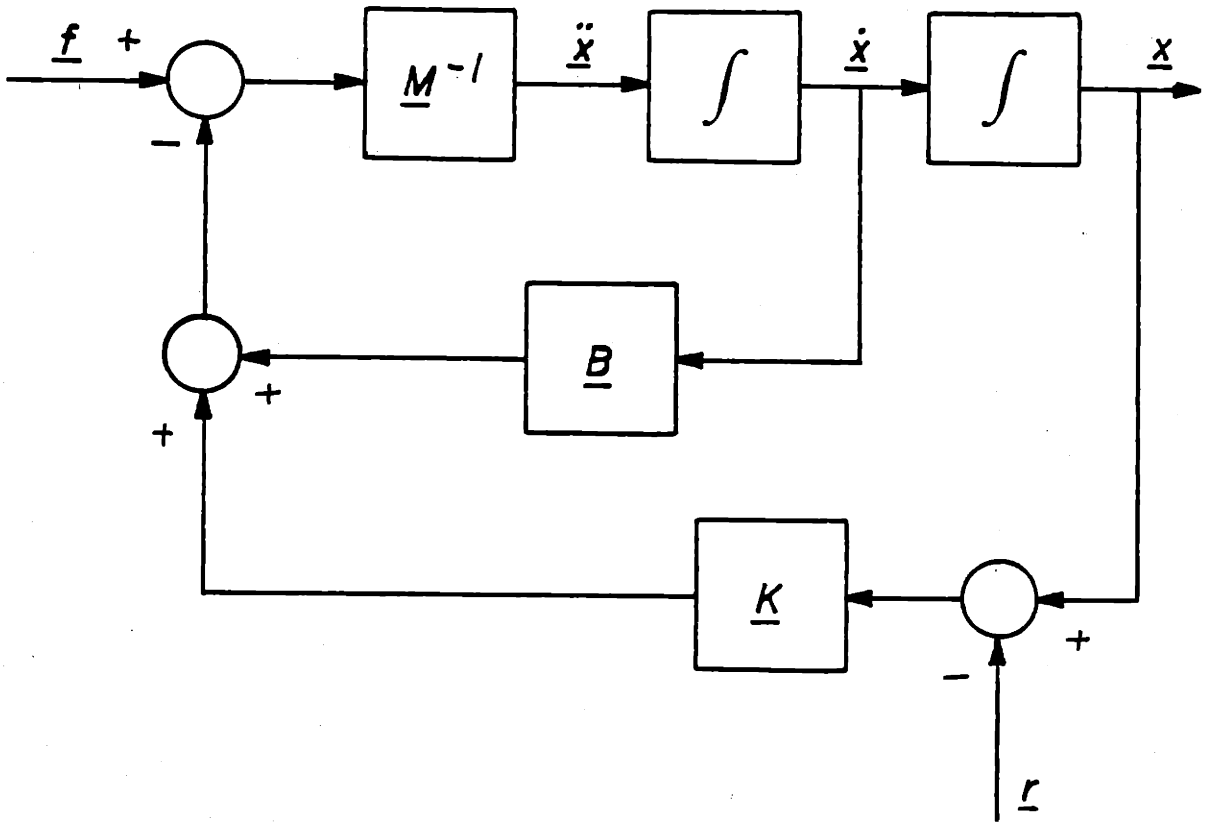


FIGURE 2-6: IMPLEMENTING REFERENCE MODEL

Note that this reference model is in task coordinates while our manipulator system is linear in joint coordinates. Thus, a coordinate transformation will be necessary and will cause problems, as will be seen later.

## 2.6 CONCLUSION

Now that some of the necessary preliminary blocks have been examined, they can be integrated. The system must look something like Fig. 2-7. If the controller drives the error, $\underline{e}$, to zero, then we have the desired position, $\underline{x}_d$, equal to the actual position, $\underline{x}$. This structure will be examined much more closely in Chapter 3.. One of the problems that will be addressed is the effect on system stability of having a coordinate transformation within the loop of a linear system. We have this coordinate transformation because we choose a reference model which was linear and time-invariant when expressed in a coordinate system other than joint coordinates.

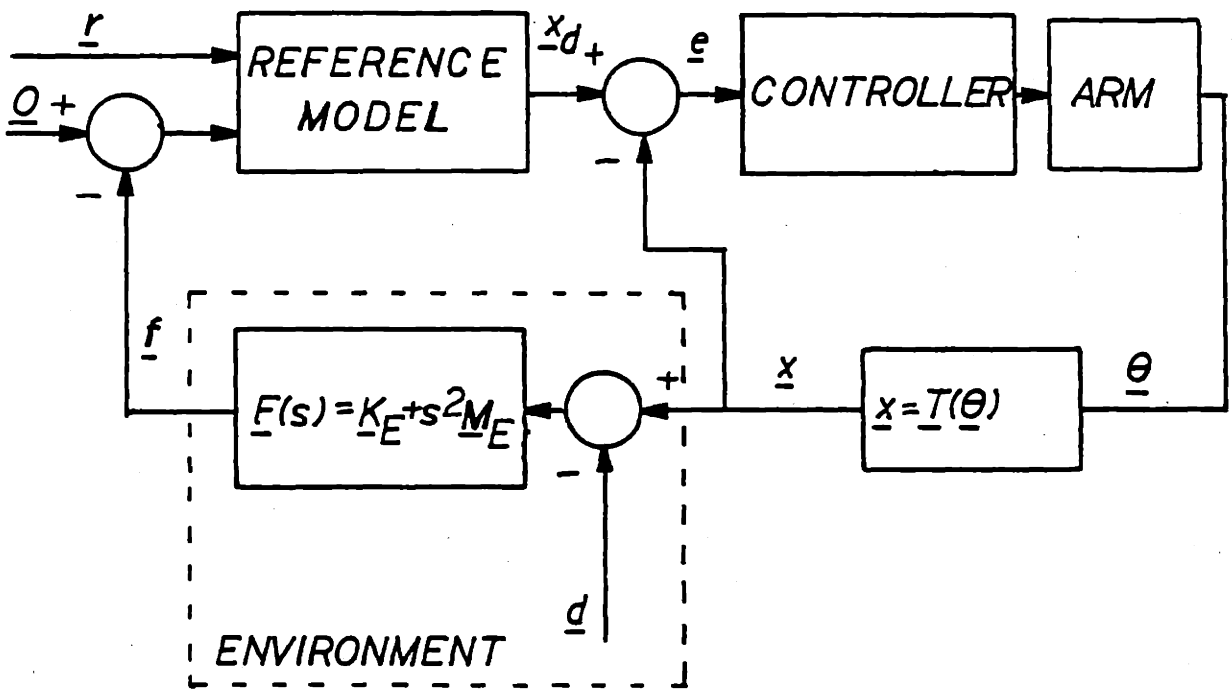


FIGURE 2-7: IMPEDANCE CONTROL SYSTEM

# 3. A LINEAR APPROACH TO IMPEDANCE CONTROL

## 3.1 Introduction

In this chapter, a method for the design of an impedance control system is developed. A linear controller structure is first presented with a general undetermined compensator. A particular choice for the compensator is chosen, namely a tracking regulator, as this allows the use of a variety of existing techniques for compensator design. Obviously, we do not pick a compensator soley on the basis of ease of design, so it must be shown that this compensator actually works and is stable under a variety of operating conditions. This is done through the use of a standard normed robustness test used in a not-so-standard way.

From this robustness test the difficulty of introducing coordinate transformations into the control loop is demonstrated and a method for partly overcoming this difficulty is shown.

## 3.2 Position Regulator for Impedance Control

We can redraw the block diagram of Fig. 2-7 as Fig. 3-1, where a coordinate transformation has been moved out from the controller and shown explicity. We can verify the validity of this structure by examining what happens if the error, $\underline{e}$, goes to zero. Then $\underline{\theta} = \underline{\theta}_d$, $\underline{x} = \underline{x}_d$, and our manipulator is at the desired position.

We can see from Fig. 3-1 that the controller is acting as a

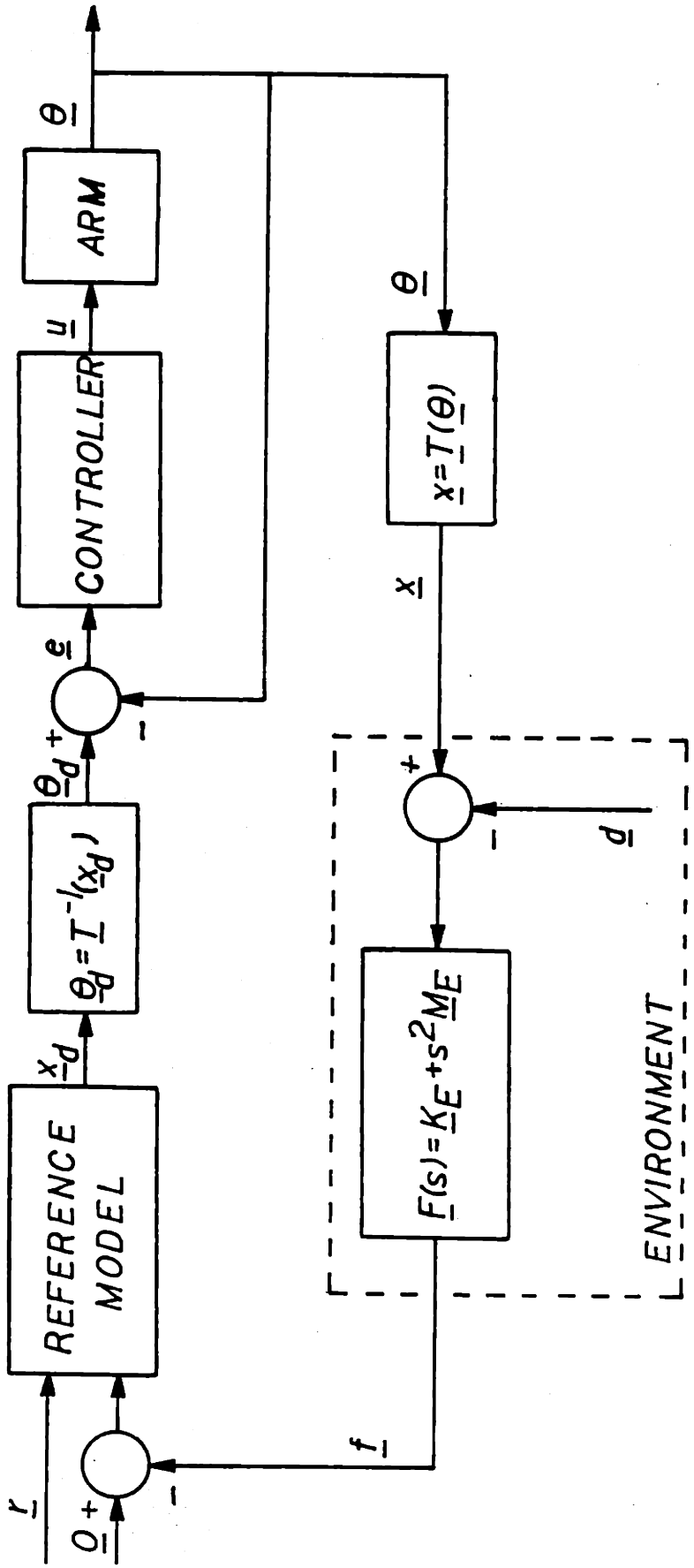


FIGURE 3-1: IMPEDANCE CONTROL SYSTEM

tracking regulator, trying to keep $\underline{\theta}$ close to $\underline{\theta}_d$. Furthermore, there are no coordinate transformations involved, simplifying the controller design. Any of a number of methods for designing the controller can be used, such as Linear-Quadratic-Gaussian or a frequency domain Bode plot approach, depending on the exact manipulator and its model.

Again looking at Fig. 3-1, we can see that the function $\underline{\theta}_d = \underline{T}^{-1}(\underline{x})$ is required. Inverting the function $\underline{T}(\underline{\theta})$ is extremely difficult to do in real time (Hewit and Burdess 1980) and it would be best to avoid it. However, we have a way out: we can take advantage of the fact that $\underline{e}$ should be close to zero (for a good controller).

$$\underline{e} = \underline{\theta}_d - \underline{\theta} = \underline{T}^{-1}(\underline{x}_d) - \underline{\theta} = \underline{T}^{-1}\underline{\theta}(\underline{x}_d + (\underline{x}-\underline{x}_d) - (\underline{x}-\underline{x}_d)) - \underline{\theta}$$
$$= \underline{T}^{-1}(\underline{x}) - \underline{J}^{-1}(\underline{\theta})(\underline{x} - \underline{x}_d) - \underline{\theta} = \underline{J}^{-1}(\underline{\theta})[\underline{x}_d - \underline{T}(\underline{\theta})]. \qquad (3\text{-}1)$$

The use of this approximation is shown in Fig. 3-2.

Thus, in Fig. 3-2, we now have an impedance control that, assuming stability, has good performance. This is guaranteed due to the tracking regulator, as explained previously. The stability issue will be studied in Section 3.3.

In order to examine the loops involved, we will need a linearized version of the system in Fig. 3-2, shown in Fig. 3-3. The command input to the reference model, $\underline{r}$, and the disturbance due to the environment, $\underline{d}$, have been supressed as we will be examining only the loops for stability. Reference and disturbance inputs have no effect on system stability, for linear systems. The reference model, $\underline{M}(s)$, represents the

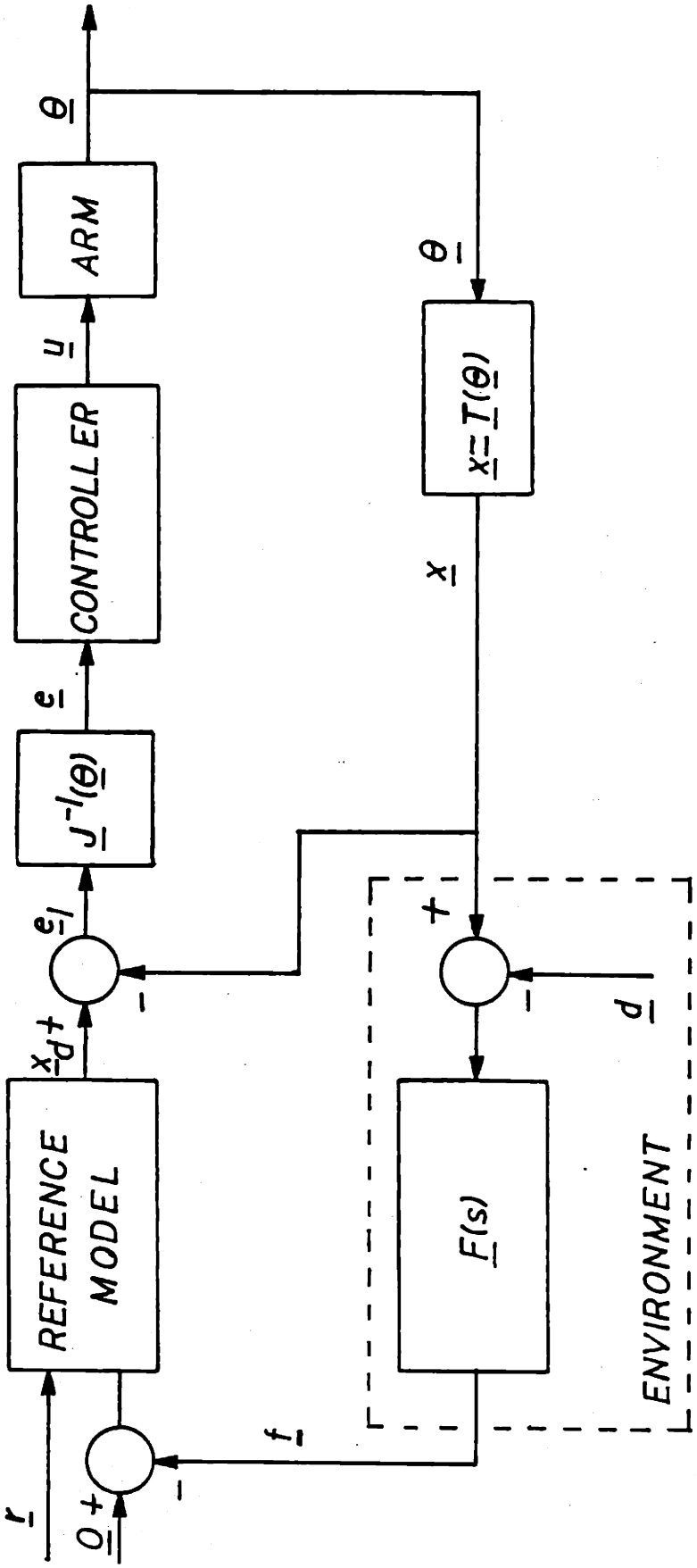


FIGURE 3-2: IMPEDANCE CONTROL SYSTEM WITHOUT $T^{-1}(x)$

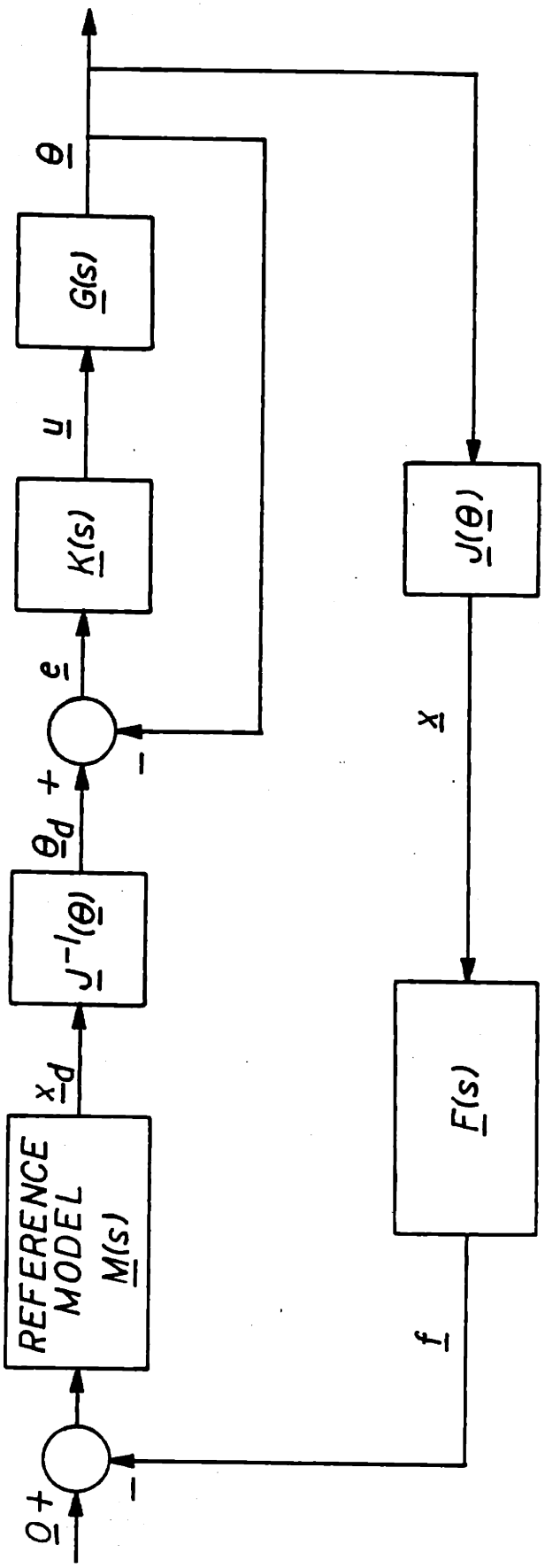


FIGURE 3-3: LINEARIZED IMPEDANCE CONTROL SYSTEM

desired transfer function from measured force to desired position, in work-space coordinates. From section 2.5, we have

$$\underline{M}(s) \doteq [\underline{M}s^2 - \underline{B}s + \underline{K}]^{-1} \quad \underline{M}, \underline{B}, \underline{K} \geq \underline{0}. \tag{3-2}$$

The environment is modeled as $\underline{F}(s)$, representing an approximation for the measured force in response to movements of the manipulator. From section 2.3,

$$\underline{F}(s) \doteq \underline{K}_E + s^2\underline{M}_E \qquad \underline{K}_E, \underline{M}_E \geq 0. \tag{3-3}$$

Recall that $\underline{K}_E$ and $\underline{M}_E$ will not be known to the controller and will not be constant.

The manipulator model, developed in section 2.4, is represented by the transfer matrix $\underline{G}(s)$, and the compensator transfer matrix for the tracking regulator is denoted $\underline{K}(s)$. Thus, the loop transmission of the position (inner) loop is $\underline{G}(s)\underline{K}(s)$. Define $\underline{H}(s)$ to be the closed-loop transfer matrix of the tracking regulator, i.e.,

$$\underline{H}(s) \doteq \underline{G}(s)\underline{K}(s)\,[\underline{I} - \underline{G}(s)\underline{K}(s)]^{-1} \tag{3-4}$$

$\underline{H}(s)$ should look like the identity matrix for low frequencies, and we expect its singular values to look similar to Fig. 3-4. In fact, if the tracking regulator does a good job, then $\underline{H}(s)$ should be diagonal (or nearly diagonal). Fig. 3-5 shows the system with $\underline{H}(s)$, and Fig. 3-6 shows the system for low frequencies, where the assumption $\underline{H}(jw) \tilde{=} \underline{I}$ is made.

The system shown in Fig. 3-6 is stable, as we expect it to be. If the loop were not stable, we made a mistake in specifying $\underline{M}(s)$, since it is performing exactly as specified. Thus, the low-frequency approximation is stable, and we wish to know

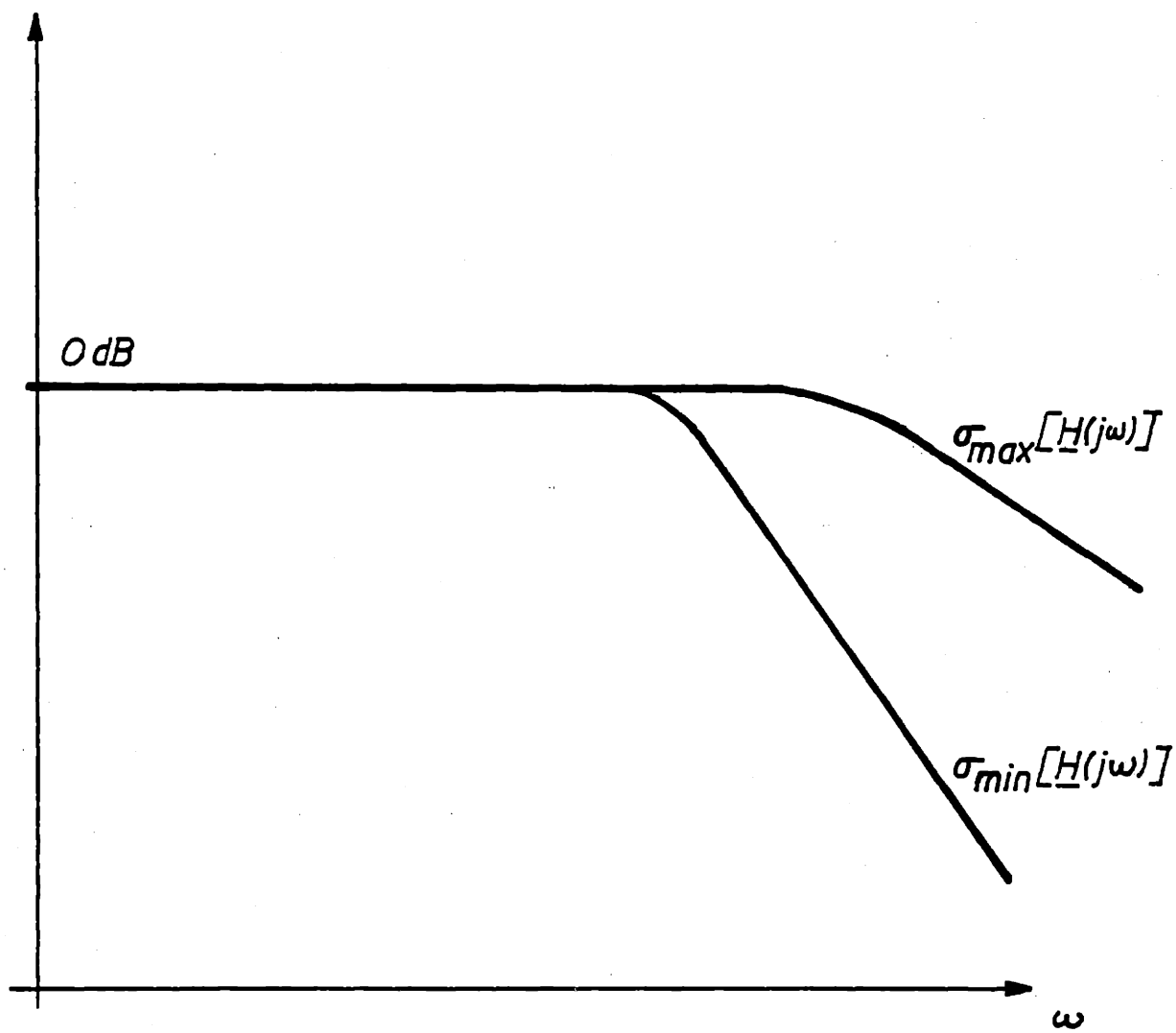


FIGURE 3-4: SINGULAR VALUES OF $\underline{H}(j\omega)$

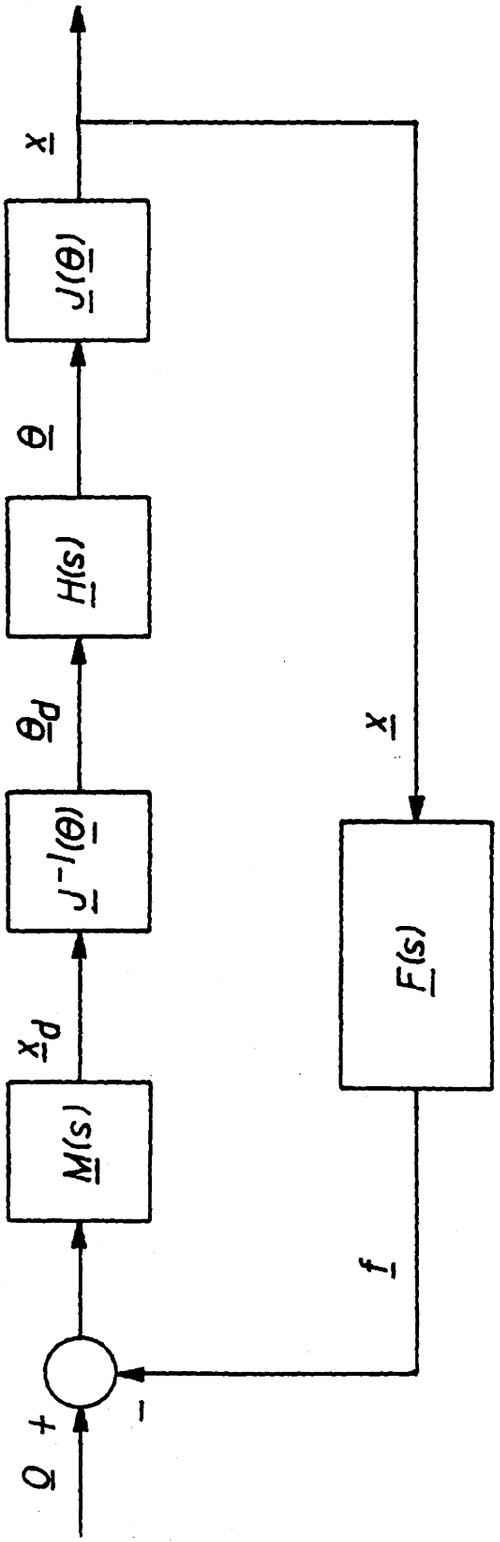


FIGURE 3-5: LOOP FOR ALL FREQUENCIES

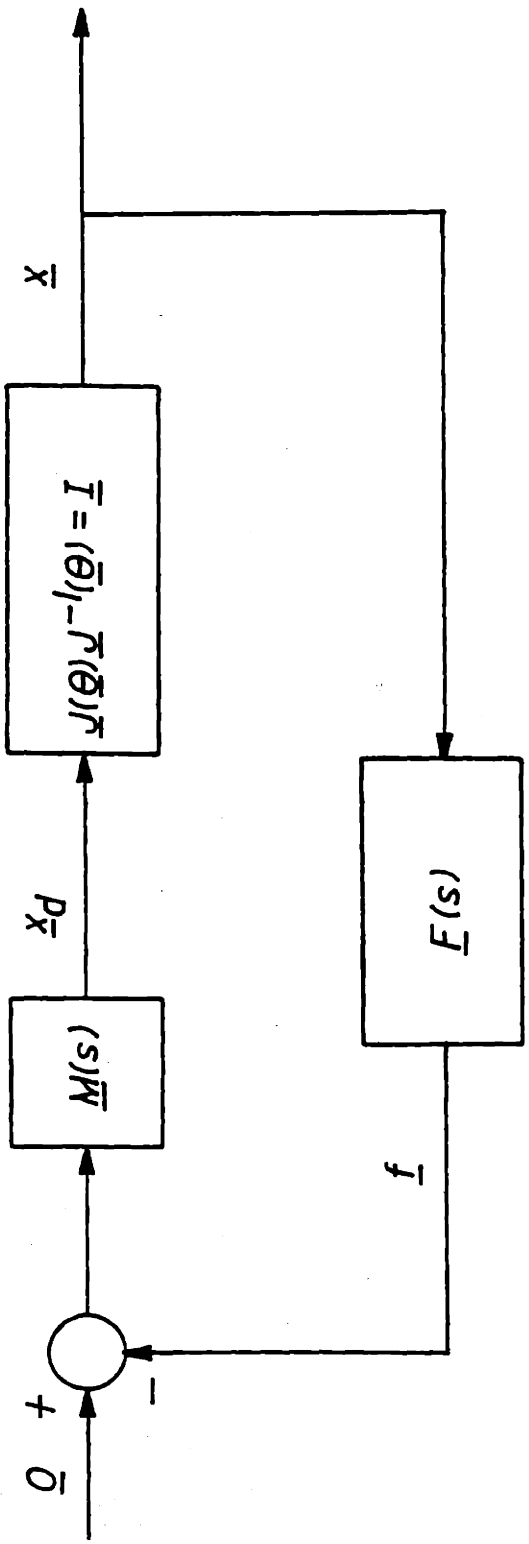


FIGURE 3-6: LOOP FOR LOW FREQUENCIES

if the general system (Fig. 3-5) is stable. This will be the subject of the next section.

## 3.3 Robustness Analysis

This section will attempt to verify the stability of the system of Fig. 3-3 through the use of a normed robustness test. For a derivation and more complete description of robustness tests, see Lehtomaki (1981).

First, the robustness test to be used will be stated. Consider the system shown in Fig. 3-7. P(s) represents the nominal open loop system and $\underline{L}(s)$ represents a perturbation on that nominal system. Assume that the nominal system is closed loop stable, i.e. that the entire system in Fig. 3-7 is stable with $\underline{L}(s) = \underline{I}$. Then the system is stable if

$$\sigma_{max}[\underline{L}(s) - \underline{I}] < \sigma_{min}[\underline{I} + \underline{P}^{-1}(s)]. \qquad (3\text{-}5)$$

If we let $\underline{P}(s) = \underline{M}(s)\underline{F}(s)$ and $\underline{L}(s) = \underline{J}(\theta)\underline{H}(s)\underline{J}^{-1}(\theta)$ then we can use this test on the system of Fig. 3-5, since we know that the system is stable for $\underline{L}(s) = \underline{I}$, or $\underline{H}(s) = \underline{I}$.

For illumination, consider a one-dimensional case, where

$$M(s) = \frac{1}{ms^2 + bs + k}$$

$$F(s) = k_e + s^2 m_e$$

$$H(s) = \frac{1}{\tau s + 1} \qquad (3\text{-}6)$$

Because we are dealing with scalars, J and $J^{-1}$ cancel and we have

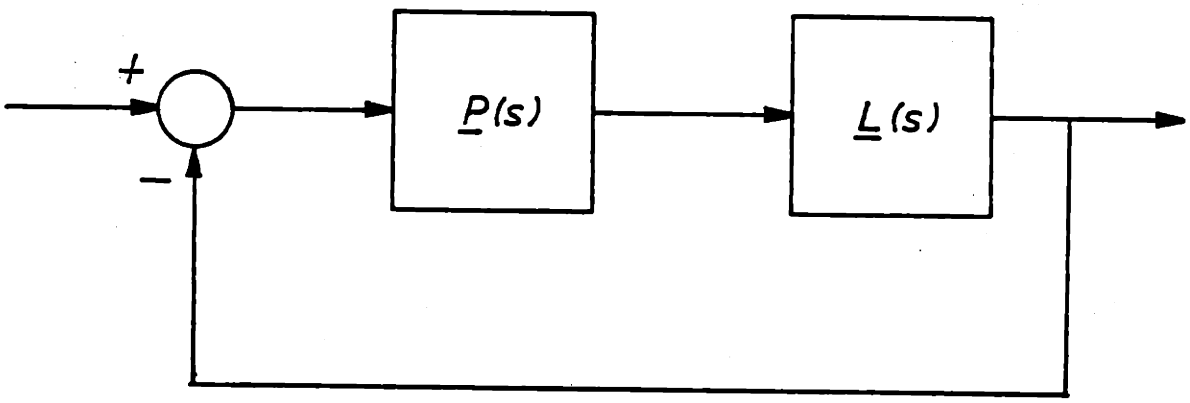


FIGURE 3-7: FEEDBACK LOOP FOR ROBUSTNESS TEST

$$\sigma_{min}[1 + P^{-1}(s)] = \frac{(m + m_e)s + bs^2 + (k + k_e)}{m_e s^2 + k_e} \qquad (3\text{-}7)$$

$$\sigma_{max}[H(s) - 1] = \frac{\tau s}{\tau s + 1} \qquad (3\text{-}8)$$

Fig. 3-8 shows a representative plot of those quantities. There are several important features of this figure. Note that $\sigma_{max}[H(s) - 1]$ is much less than 1 at low frequencies and approaches 1 as the frequency increases. The fact that this plot has no overshoot in it is an artifact of the one-pole form selected for H(s) above. This will be important, as will be seen in section 3.5. Next, note that $\sigma_{min}[1 + P^{-1}(s)]$ is greater than 1 at DC and at high frequencies, because m, $m_e$, k, $k_e$ are all greater than zero.

Thus, for the situation depicted in Fig. 3-8, the impedance control system will be closed loop stable: The "perturbation" represented by the tracking regulator's closed loop response is small enough to not affect system stability.

As this procedure is generalized to the multi-variable case, the Jacobian matrix remains in and causes difficulty as will be shown next.

Let the reference model be represented by

$$\underline{M}(s) = [\underline{M}s^2 + \underline{B}s + \underline{k}]^{-1} \; ; \; \underline{M} = m\underline{I} \geq 0, \; \underline{B} \geq 0, \; \underline{K} \geq 0. \qquad (3\text{-}9)$$

and the environment be represented by

$$\underline{F}(s) = \underline{K}_E + s^2\underline{M}_E \; ; \; \underline{M}_E = m_E\underline{I} \geq \underline{0}; \; \underline{K}_E \geq \underline{0}, \qquad (3\text{-}10)$$

Now, the system of Fig. 3-5 is stable if

$$\sigma_{max}[\underline{J}(\underline{\theta})\underline{H}(s)\underline{J}^{-1}(\underline{\theta}) - \underline{I}] < \sigma_{min}[\underline{I} + [\underline{M}(s)\underline{F}(s)]^{-1}]. \qquad (3\text{-}11)$$

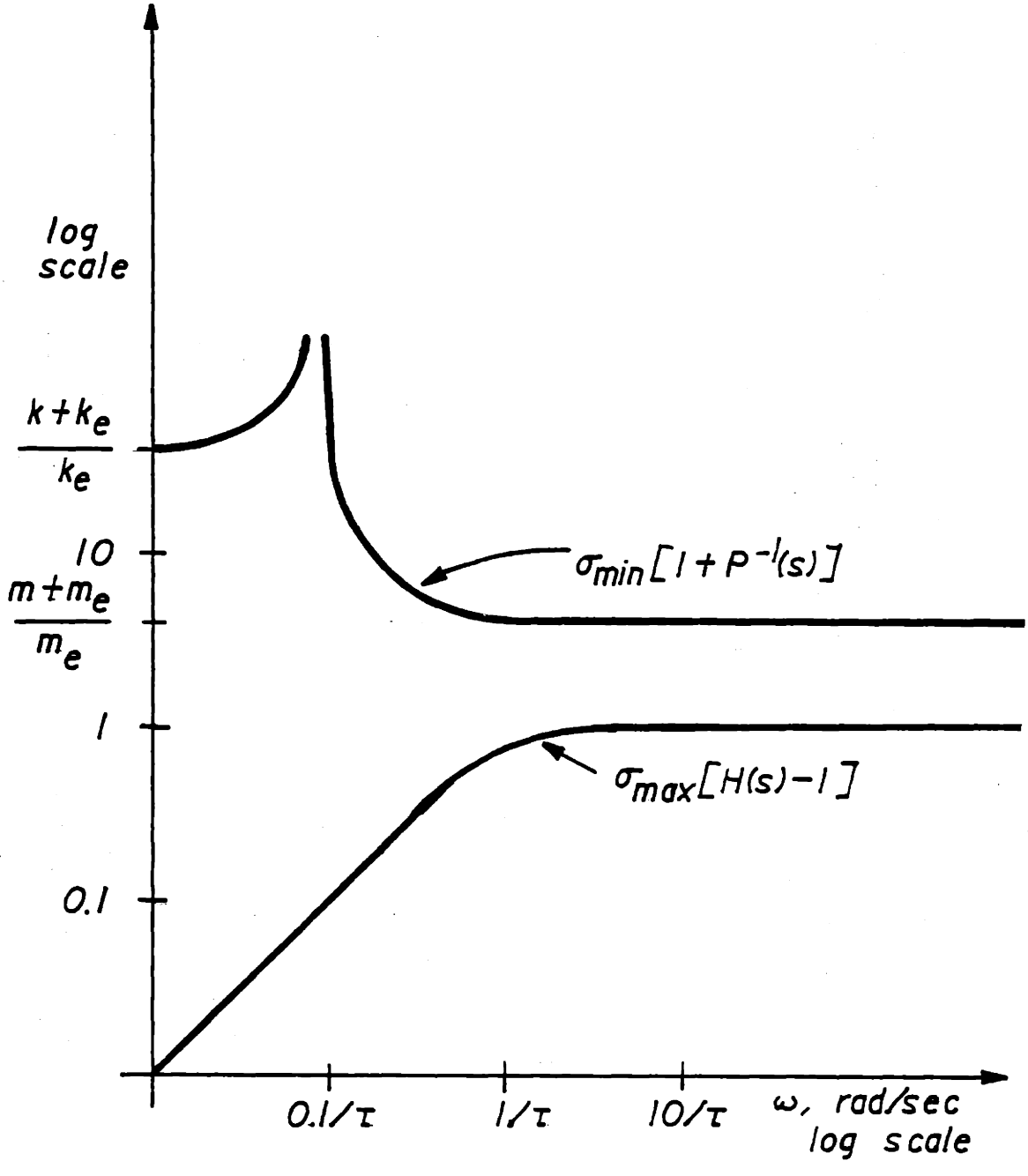


FIGURE 3-8: ROBUSTNESS OF SIMPLE SCALAR CASE

Now,

$$\sigma_{max}[\underline{J}(\underline{\theta})\underline{H}(s)\underline{J}^{-1}(\underline{\theta}) - I] = \sigma_{max}[\underline{J}(\underline{\theta})[\underline{H}(s) - \underline{I}]\ \underline{J}^{-1}(\underline{\theta})] \tag{3-12}$$

and since $\sigma_{max}(\underline{A})$ is a norm, we have

$$\sigma_{max}[\underline{J}(\underline{\theta})\underline{H}(s)\underline{J}^{-1}(\underline{\theta}) - \underline{I}] \leq \sigma_{max}[\underline{J}(\underline{\theta})] \cdot \sigma_{max}[\underline{J}^{-1}(\underline{\theta})] \cdot \sigma_{max}[\underline{H}(s) - \underline{I}]. \tag{3-13}$$

Utilizing the fact that $\sigma^{-1}_{max}(\underline{A}) = \sigma_{min}(\underline{A}^{-1})$, we obtain

$$\sigma_{max}[\underline{J}(\underline{\theta})\underline{H}(s)\underline{J}^{-1}(\underline{\theta}) - \underline{I}] \leq \left\{ \frac{\sigma_{max}[\underline{J}(\underline{\theta})]}{\sigma_{min}[\underline{J}(\underline{\theta})]} \right\} \sigma_{max}[\underline{H}(s) - \underline{I}] \tag{3-14}$$

The quantity in braces is given a special name (Strang 1980); it is called the <u>condition number</u> of $\underline{J}(\underline{\theta})$, denoted here by $\text{cond}_{\vee}(\underline{J}(\underline{\theta}))$. It represents a measure of the difficulty of inversion of $\underline{J}(\underline{\theta})$ and gives the maximum amplification of the norm of a matrix undergoing a coordinate transformation induced by $\underline{J}(\underline{\theta})$. Our test for the stability of Fig. 3-5 is now

$$\sigma_{max}[\underline{H}(s) - \underline{I}] \cdot \text{cond}(\underline{J}(\underline{\theta})) < \sigma_{min}[\underline{I} + (\underline{M}(s)\underline{F}(s))^{-1}]. \tag{3-14}$$

A plot of this, analogous to Fig. 3-8, is shown in Fig. 3-9. Let $\omega_1$ denote the frequency of the peak in $\sigma_{min}[\underline{I} + (\underline{M}(s)\underline{F}(s))^{-1}]$ and $\omega_2$ denote the breakpoint for $\sigma_{max}[\underline{H}(s) - \underline{I}]$. From Fig. 3-9 we can then obtain some approximate rules for stability of our impedance control system.

<u>Remark 1</u>: We must have sufficient separation between the two curves A and B in Fig. 3-9 to allow for the condition

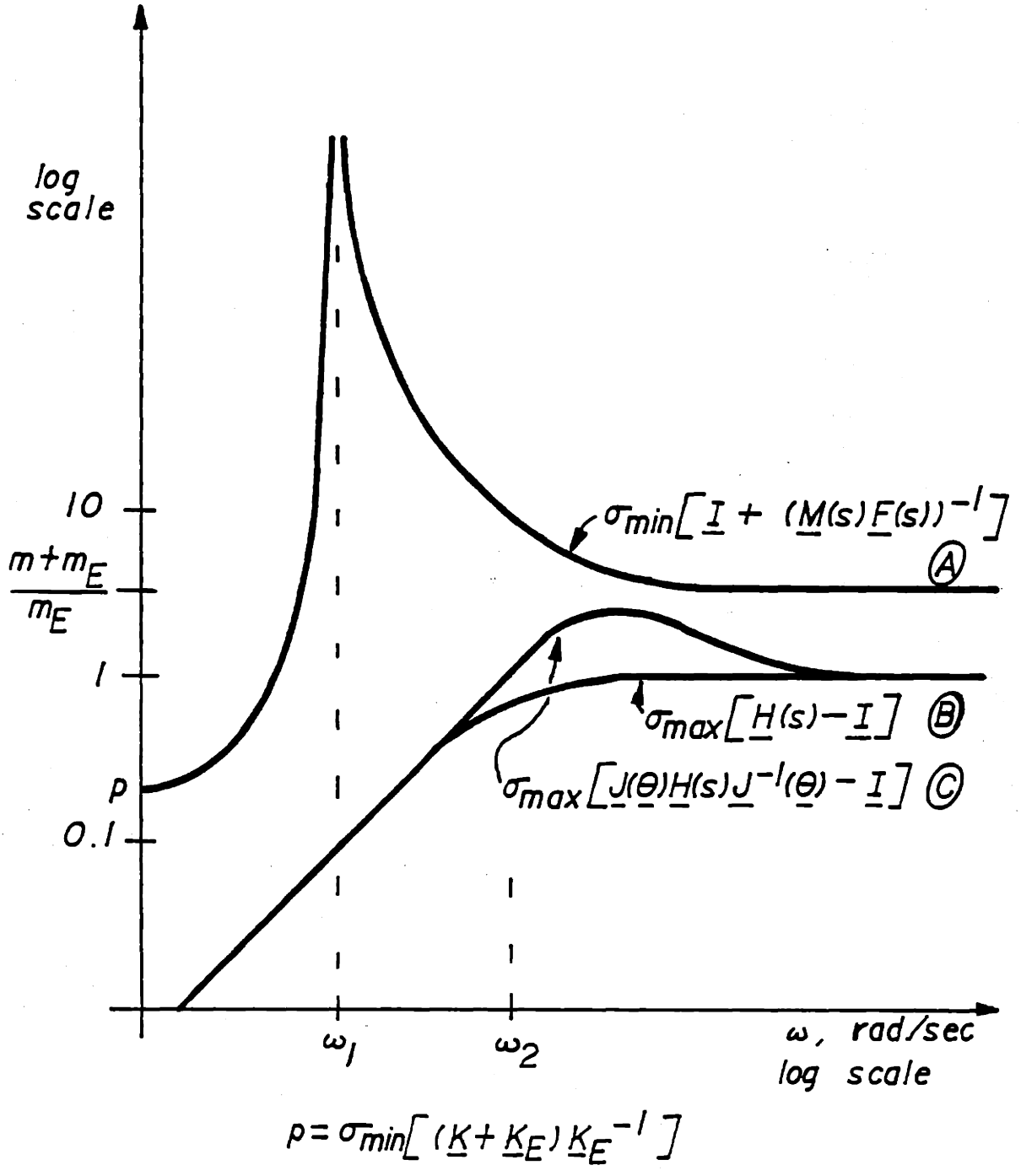


FIGURE 3-9: MULTIVARIABLE ROBUSTNESS TEST

number of $\underline{J}(\underline{\theta})$; we must allow for the largest expected value so that curve C remains below curve A. Note that this margin is only required for the middle frequencies.

Remark 2: If $\omega_2 >> \omega_1$ and the above conditions are satisfied, then we will be safe for all values of $\underline{K}_E$, as $\underline{K}_E$ only impacts the low frenquency behavior of curve A. This is saying that the robot dynamics should be significantly faster than the model dynamics. This makes good intuitive sense, as we don't wish to command the manipulator to move faster than it is capable.

Remark 3: If we don't have significant separation between $\omega_1$ and $\omega_2$, we may be still safe, if $\sigma_{min}[(\underline{K} + \underline{K}_E)\underline{K}_E^{-1}]$ is large enough. This indicates that we may get into trouble if $\underline{K}_E$ is very "large". As will be seen in chapter 4, a large $\sigma_{max}(\underline{K}_E)$ can cause instability. Fig. 3-10 shows such a situation.

Since this robustness test is only a sufficient condition for stability and not a necessary one, we expect the requirements it gives to be somewhat conservative. We could also use any of a number of other forms of normed robustness tests, but they do not appear to give the intuitive insight that the one used here does. The next section will attempt to present some conditions under which the conservativeness of the test can be reduced and thus lessen the seriousness of the coordinate transformation involved.

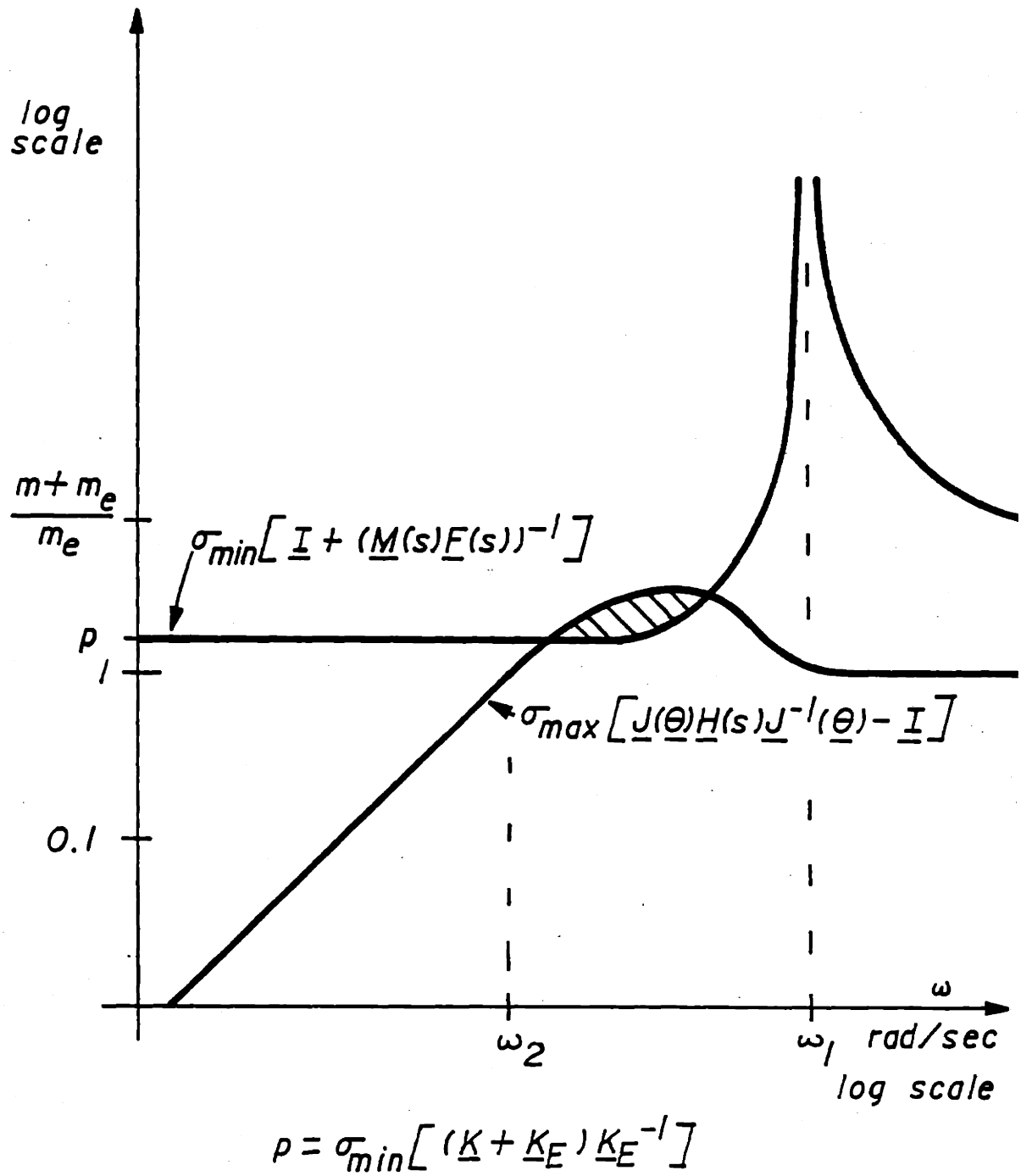


FIGURE 3-10: MULTIVARIABLE ROBUSTNESS TEST THAT FAILS

## 3.4 Some Less Conservative Bounds

The last section rested heavily on the fact

$$|| \underline{J}[\underline{H}(s) - \underline{I}]\underline{J}^{-1}|| \leq \text{cond } (\underline{J}) \; || \underline{H}(s) - \underline{I} \; ||. \tag{3-15}$$

and used this to derive a sufficient condition for the stability of the impedance control system:

$$\sigma_{min}[\underline{I} + (\underline{M}(s)\underline{F}(s))^{-1}] > \text{cond}(\underline{J}) \cdot \sigma_{max}[\underline{H}(s) - \underline{I}]. \tag{3-16}$$

In order to get a feel for the condition number of $\underline{J}(\underline{\theta})$, we can calculate it for our simple two-link manipulator for various angles. Consider the manipulator of Fig. 2-2. Since it does not affect the condition number, d = 1 will be assumed (d just scales all of the singular values). We have

$$\text{cond } (\underline{J}) = \frac{\sigma_{max}(\underline{J})}{\sigma_{min}(\underline{J})} \tag{3-17}$$

and

$$\sigma_{max}(\underline{J}) = \lambda_{max}^{1/2}[\underline{J}^H\underline{J}] \; ; \quad \sigma_{min}(\underline{J}) = \lambda_{min}^{1/2}[\underline{J}^H\underline{J}]. \tag{3-18}$$

$$\underline{J}^H\underline{J} = \begin{bmatrix} \cos\phi_1 & -\sin\phi_1 \\ \cos\phi_2 & -\sin\phi_2 \end{bmatrix} \begin{bmatrix} \cos\phi_1 & \cos\phi_2 \\ -\sin\phi_1 & -\sin\phi_2 \end{bmatrix}$$

$$= \begin{bmatrix} 1 & \cos(\phi_1 - \phi_2) \\ \cos(\phi_1 - \phi_2) & 1 \end{bmatrix} \tag{3-19}$$

Notice that the matrix $\underline{J}^H\underline{J}$ (and thus the singular values) are a function of $\phi_1 - \phi_2$ which is just the angle of deflection of the central link. Thus curves of equal singular values are circles centered at the origin, since radius is only a function of

central angle. We have

$$\sigma_{min}(\underline{J}) = \left[\frac{2 - \sqrt{3 + \cos^2(\phi_1 - \phi_2)}}{2}\right]^{1/2} \qquad (3\text{-}20)$$

$$\sigma_{max}(\underline{J}) = \left[\frac{2 + \sqrt{3 + \cos^2(\phi_1 - \phi_2)}}{2}\right]^{1/2} \qquad (3\text{-}21)$$

Due to the cosine-squared term, the condition number of $\underline{J}$ is equal for $\phi_1 - \phi_2 = \alpha$ and $\phi_1 - \phi_2 = 180 - \alpha$, $0 \leq \alpha \leq 180°$. Table 3-1 lists the singular values as a function of angle. In Table 3-1,

$r(\alpha)$ = distance of end-effector from the origin for $\phi_1 - \phi_2 = \alpha$

$r(180 - \alpha)$ = distance of end-effector from origin for

$$\phi_1 - \phi_2 = 180 - \alpha$$

$\underline{J}(\alpha)$ = Jacobian matrix for $\phi_1 - \phi_2 = \alpha$. Fig. 3-11 shows these values as circles of equal condition numbers.

For example, if we allow the end-effector of the manipulator to come to within 0.17 units of the origin, the condition number of $\underline{J}$ could reach 23.0. Therefore we must allow a factor of 23 between our two singular value curves (A and B in Fig. 3-9). This puts a very stringent requirement on the speed of our manipulator system. $\omega_2$ must be very high to give us the required separation (perhaps two decades between model and manipulator- quite a waste of bandwidth.). Thus, we would like to reduce the conservativeness of our robustness test. This can be done as will be shown next.

Suppose $\underline{H}(s) = \lambda(s)\underline{I}$, $\lambda(s)$ a scalar function of s. Then

| $\alpha$ | $r(\alpha)$ | $180^\circ - \alpha$ | $r(180^\circ - \alpha)$ | $\sigma_{max}[\underline{J}(\alpha)]$ | $\sigma_{min}[\underline{J}(d)]$ | $cond(\underline{J}(\alpha))$ |
|---|---|---|---|---|---|---|
| $0^\circ$ | 2.0000 | 180 | 0.0000 | 1.4142 | 0.0000 | $\infty$ |
| 1 | 1.9999 | 179 | 0.0175 | 1.4142 | 0.0062 | 229.2 |
| 2 | 1.9997 | 178 | 0.0349 | 1.4142 | 0.0123 | 114.6 |
| 3 | 1.9993 | 177 | 0.0524 | 1.4141 | 0.0185 | 76.42 |
| 4 | 1.9988 | 176 | 0.0698 | 1.4140 | 0.0247 | 57.32 |
| 5 | 1.9981 | 175 | 0.0872 | 1.4139 | 0.0308 | 45.87 |
| 10 | 1.9924 | 170 | 0.1743 | 1.4129 | 0.0615 | 22.99 |
| 15 | 1.9829 | 165 | 0.2611 | 1.4112 | 0.0917 | 15.39 |
| 20 | 1.9696 | 160 | 0.3473 | 1.4090 | 0.1214 | 11.61 |
| 25 | 1.9526 | 155 | 0.4329 | 1.4062 | 0.1503 | 9.36 |
| 30 | 1.9319 | 150 | 0.5176 | 1.4029 | 0.1782 | 7.87 |
| 35 | 1.9074 | 145 | 0.6014 | 1.3993 | 0.2050 | 6.83 |
| 40 | 1.8794 | 140 | 0.6840 | 1.3953 | 0.2303 | 6.06 |
| 45 | 1.8479 | 135 | 0.7654 | 1.3912 | 0.2541 | 5.47 |
| 50 | 1.8126 | 130 | 0.8452 | 1.3870 | 0.2762 | 5.02 |
| 55 | 1.7740 | 125 | 0.9235 | 1.3829 | 0.2962 | 4.67 |
| 60 | 1.7321 | 120 | 1.0000 | 1.3789 | 0.3140 | 4.39 |
| 65 | 1.6868 | 115 | 1.0746 | 1.3753 | 0.3295 | 4.17 |
| 70 | 1.6383 | 110 | 1.1472 | 1.3721 | 0.3424 | 4.01 |
| 75 | 1.5867 | 105 | 1.2175 | 1.3695 | 0.3526 | 3.88 |
| 80 | 1.5321 | 100 | 1.2856 | 1.3676 | 0.3600 | 3.80 |
| 85 | 1.4746 | 95 | 1.3512 | 1.3664 | 0.3645 | 3.75 |
| 90 | 1.4142 | 90 | 1.4142 | 1.3660 | 0.3660 | 3.73 |

TABLE 3-1

CONDITION NUMBERS

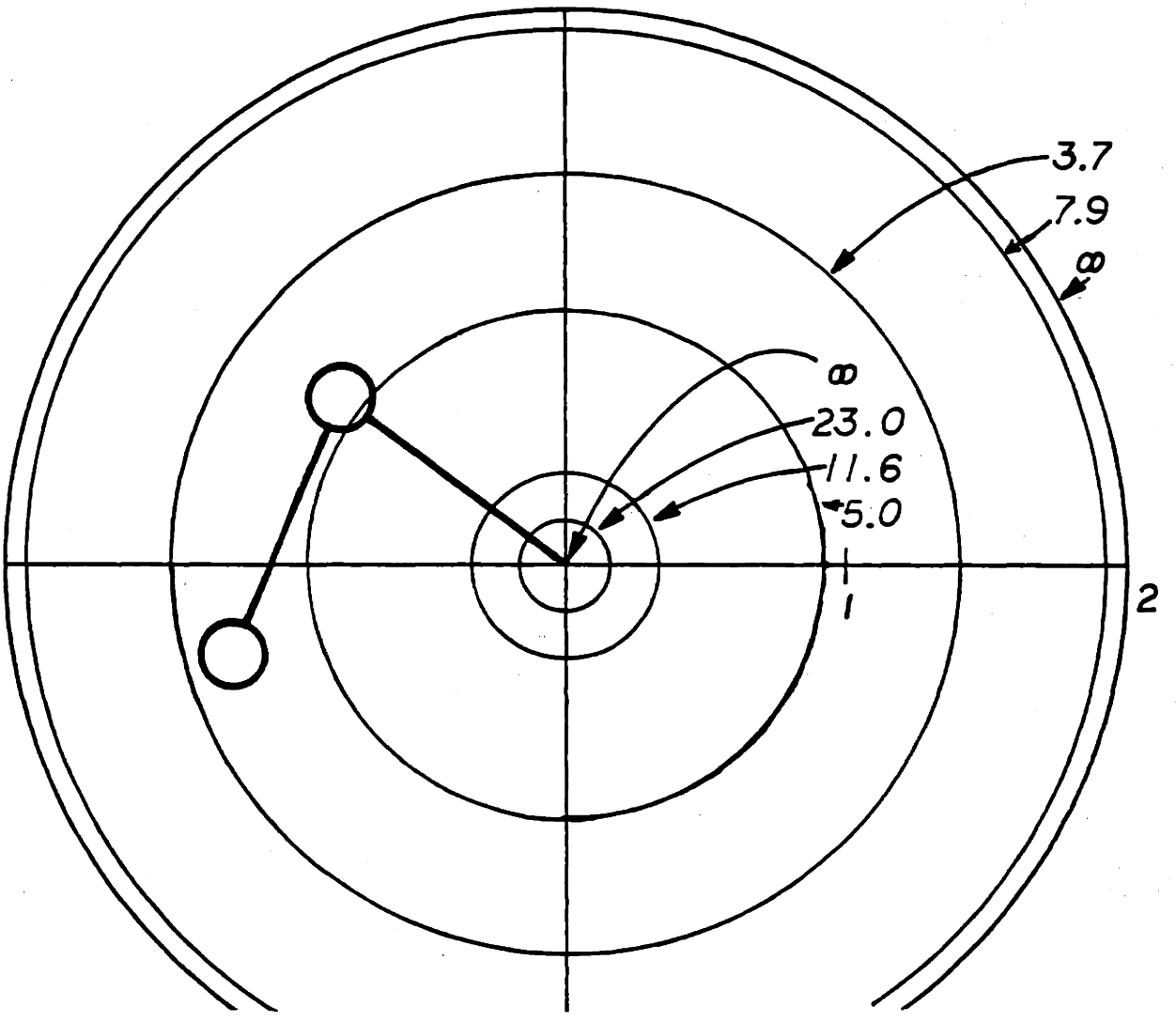


FIGURE 3-11: CONDITION NUMBERS FOR MANIPULATOR POSITIONS

$||\underline{J}(\underline{H}(s) - \underline{I})\underline{J}^{-1}|| = ||\underline{H}(s) - \underline{I}||$ because $\underline{J}$ will commute with $\underline{H}(s)$. The closer $\underline{H}(s)$ is to a diagonal matrix with equal elements, the less the effect of the coordinate transformation.

In order to be more quantitative about this, we can investigate the effect of a general matrix, $\underline{H}(s)$, which we can write as

$$\underline{H}(s) = \lambda(s)\underline{I} + \underline{B}(s). \tag{3-22}$$

This allows us to take advantage of the desirability of the $\lambda(s)\underline{I}$ term. We now have

$$||\underline{J}[\underline{H}(s) - \underline{I}]\underline{J}^{-1}|| \leq ||(\lambda(s) - 1)\underline{I}|| + ||\underline{J}\underline{B}(s)\underline{J}^{-1}|| \leq |\lambda(s) - 1| + \text{cond}(\underline{J}) \cdot ||\underline{B}(s)|| \tag{3-23}$$

This shows that if $\underline{H}(s)$ is decomposed into $\underline{H}(s) = \lambda(s)I + \underline{B}(s)$ such that $||\underline{B}(s)||$ is minimized, we can reduce the effect of the condition number on our robustness test.

As mentioned earlier (section 3.2), if the tracking regulator, $\underline{K}(s)$, does a good job, we expect $\underline{H}(s)$ to be diagonal, as commanded positions in one channel shouldn't affect another channel. Consider the 2 x 2 case (for the two-link manipulator being studied). Then

$$\underline{H}(s) = \begin{bmatrix} h_1(s) & 0 \\ 0 & h_2(s) \end{bmatrix} = \lambda(s)\underline{I} + \underline{B}(s). \tag{3-24}$$

We can decompose this so that $\underline{B}(s)$ has the smallest norm possible by inspection:

$$\underline{H}(s) = \tfrac{1}{2}\begin{bmatrix} h_1(s) + h_2(s) & 0 \\ 0 & h_1(s) + h_2(s) \end{bmatrix}$$

$$+ \tfrac{1}{2}\begin{bmatrix} h_1(s) - h_2(s) & 0 \\ 0 & h_2(s) - h_1(s) \end{bmatrix}$$

$$= \left(\tfrac{1}{2}\right)(h_1(s) + h_2(s))\,\underline{I} + \frac{h_1(s) - h_2(s)}{2}\begin{bmatrix} 1 & 0 \\ 0 & -1 \end{bmatrix} \qquad (3\text{-}25)$$

Therefore $\lambda(s) = \dfrac{h_1(s) + h_2(s)}{2}$

and $||\underline{B}(s)|| = \dfrac{h_1(s) - h_2(s)}{2}$ (3-26)

If $\underline{H}(s)$ is not quite diagonal, the off-diagonal terms will appear in $\underline{B}(s)$. If their magnitude is small compared to the magnitude of $\frac{1}{2}[h_1(s) - h_2(s)]$ they will not bother us, as they will not affect the norm of $\underline{B}(s)$. If they are not small, they will have to be added in to the norm of $\underline{B}(s)$.

Now, we know that our control system will stable if

$$\sigma_{min}[\underline{I} + (\underline{M}(s)\underline{F}(s))^{-1}] > |\lambda(s) - 1| + \text{cond}(\underline{J})\,\sigma_{max}[\underline{B}(s)] \qquad (3\text{-}27)$$

where $\lambda(s)\underline{I} + \underline{B}(s) = \underline{H}(s)$, our tracking regulator closed loop response. Thus, we can reduce the conservativeness of our original robustness test if we know something of the structure of the "error", $\underline{H}(s) - \underline{I}$. The smaller $h_1(s) - h_2(s)$ is, the less will be the amplification due to the coordinate transformation.

This suggests that we could reduce the effect of the

coordinate transformation by proper selection of $\underline{K}(s)$, which is our only control over $\underline{H}(s)$. We may now be able to use our robustness test for design rather than just analysis. Above, it was discovered that a small $|\, h_1(s) - h_2(s) \,|$ will reduce the effect of the coordinate transformation on system stability. This suggests that $h_1(s)$ and $h_2(s)$ should behave similarly, and since $\underline{H}(s) = \underline{G}(s)\underline{k}(s)[\underline{I} + \underline{G}(s)\underline{k}(s)]^{-1}$, we may be able to select $\underline{K}(s)$ to give us the form we want, namely equal frequency response in the different channels. This will form the subject of the next section.

## 3.5 Modifications Based on Robustness

The last section suggests that a "good" structure for $\underline{H}(s)$ is one in which all the channels are as similar as possible. This makes intuitive sense in another way: If the channels have significantly different bandwidths, we will be in trouble when we attempt to follow an arbitrary path in task-coordinates (cartesian coordinates), as the different servo lags (error coefficients for ramp inputs) will cause the actual path to lie to one side of the desired path.

From the last section

$$\underline{H}(s) = \begin{bmatrix} h_1(s) & 0 \\ 0 & h_2(s) \end{bmatrix} = \lambda(s)\underline{I} + \underline{B}(s). \qquad (3\text{-}28)$$

To minimize the effect of the coordinate transformation, we want $h_1(s) - h_2(s)$ to be as small as possible. Fig. 3-12

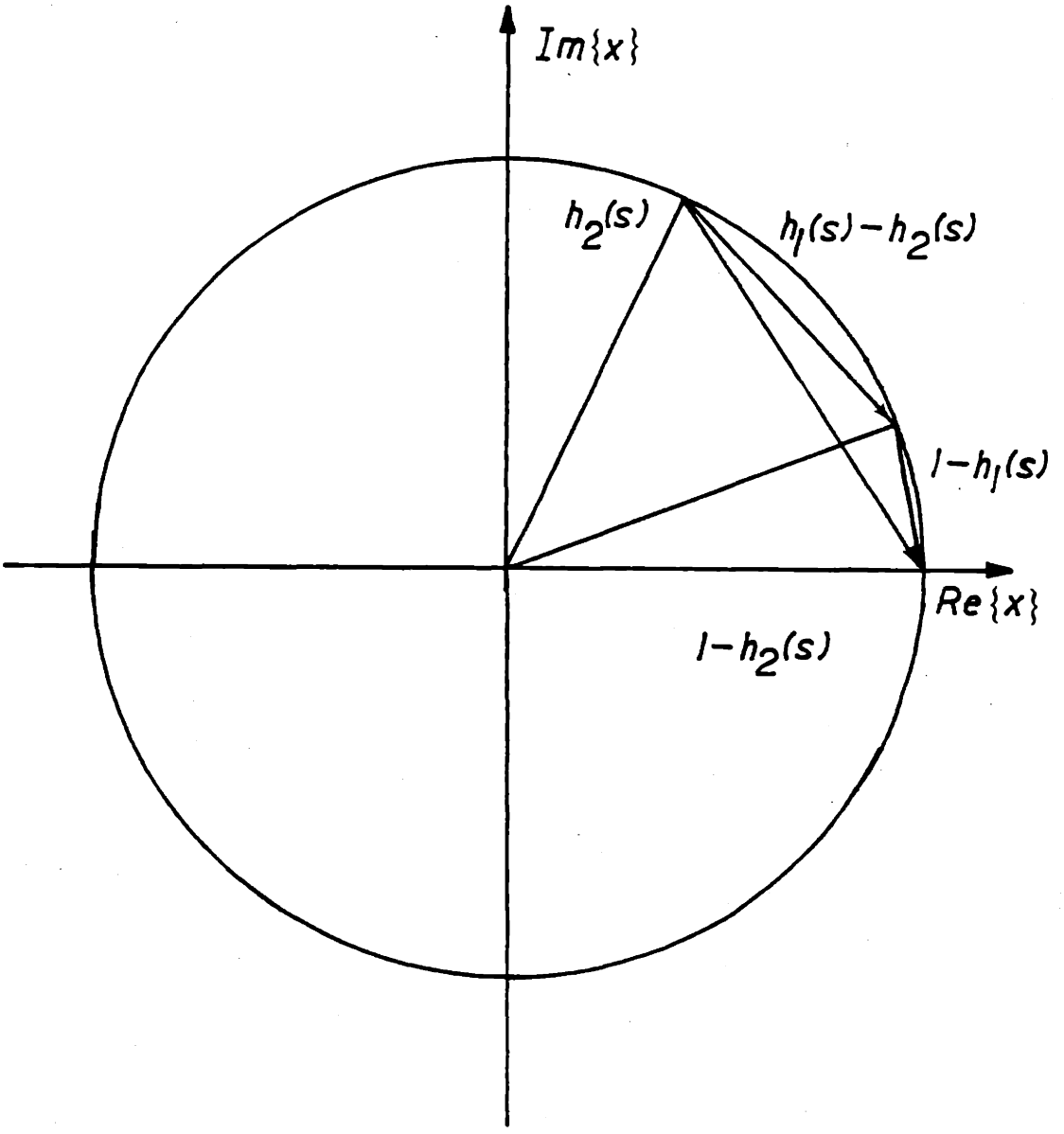


FIGURE 3-12: CALCULATION OF $h_1(s)-h_2(s)$

shows the vectors $h_1(s) - h_2(s)$, $1 - h_1(s)$, and $1 - h_2(s)$. Remember that we also want $1 - h_1(s)$ and $1 - h_2(s)$ small, as we want

$$|\lambda(s) - 1| = \left| \frac{h_1(s) + h_2(s)}{2} - 1 \right| \qquad (3\text{-}29)$$

small.

Note that

$$\left| \tfrac{1}{2}[1 - h_1(s)] + \tfrac{1}{2}[1 - h_2(s)] \right| = \frac{h_1(s) + h_2(s)}{2} \qquad (3\text{-}30)$$

The purpose of all this is that we can now see that $h_1(s)$ and $h_2(s)$ should remain in the first quadrant in order that there difference remain small. While it is true that they could both go into the second quandrant "together" [i.e. $h_1(s) = h_2(s)$], we must keep in mind that modeling errors and parameter perturbations do exist. Consider what happens if a perturbation brings $h_2(s)$ back into the first quadrant. Then $|h_1(s) - h_2(s)|$ could reach (almost) 2. Thus, by keeping both $h_1(s)$ and $h_2(s)$ in the first quadrant (at least until their magnitude has decreased significantly), we guarantee that

$$|h_1(s) - h_2(s)| < \sqrt{2}\,. \qquad (3\text{-}31)$$

(Remember that $h_1(0) = h_2(0) = 1$).

Thus, consider

$$\underline{H}(s) = \begin{bmatrix} \dfrac{1}{\tau_1 s + 1} & 0 \\ 0 & \dfrac{1}{\tau_2 s + 1} \end{bmatrix} \qquad (3\text{-}32)$$

Suppose that we manage to bring the bandwidth of the channels to within a factor of two, i.e. $\tau = \tau_1 = 2\tau_2$

$$\underline{H}(s) = \begin{bmatrix} \frac{1}{2\tau s + 1} & 0 \\ 0 & \frac{1}{\tau s + 1} \end{bmatrix} \doteq \begin{bmatrix} h_1(s) & 0 \\ 0 & h_2(s) \end{bmatrix} \qquad (3\text{-}33)$$

The largest deviation $h_1(j\omega) - h_2(j\omega)$ occurs at $\omega = \frac{1}{\tau\sqrt{2}}$ and is of magnitude

$$d \doteq \left| h_1(j\omega) - h_2(j\omega) \right| = \left| \frac{1}{\tau\omega j + 1} - \frac{1}{2\tau j\omega + 1} \right|$$

$$= \left| \frac{\tau j\omega}{(\tau j\omega + 1)(2\tau j\omega + 1)} \right| \qquad (3\text{-}34)$$

Evaluating at $\omega = \frac{1}{\tau\sqrt{2}}$

$$|d| = 1/3 \quad . \qquad (3\text{-}35)$$

Thus, for the system, we have

$$|| \underline{J}(\underline{H}(s) - \underline{I})\underline{J}^{-1} || \leq |\lambda(s) - 1| + \text{cond}(\underline{J}) \cdot || \underline{B}(s) || \qquad (3\text{-}36)$$

or

$$|| \underline{J}(\underline{H}(s) - \_)\_^{-1} || \leq \left| \tfrac{1}{2}(h_1(s) + h_2(s)) - 1 \right| + \text{cond}(\underline{J}) \tfrac{1}{2} \left| h_1(s) - h_2(s) \right|$$

$$\leq \sqrt{2} + \left(\tfrac{1}{6}\right) \text{cond}(\underline{J}) \qquad (3\text{-}37)$$

where the $\sqrt{2}$ is approximate (the actual upper bound will be smaller and thus give a tighter bound). The main point is that now the Jacobian, $\underline{J}$, whose condition number we may allow to go to 10 or 20 is much reduced in its effect on our system's stability.

Therefore, to utilize this new information, we must simply bring the two channels to approximately the same bandwidth with a single dominant pole—other dynamics must be at a higher frequency. This is done through proper selection of the compen-

sator $\underline{K}(s)$. In the case of the Rhino, discussed in chapter 4, this is relatively straightforward.

## 3.6 Conclusion

This chapter has presented a method for implementing impedance control. The purpose of this analysis was to provide analytical justification for the intuitive introduction of the method and to provide some information about the proper compensator. It was shown that the closed loop response of the tracking regulator should be as close to $\underline{I}\lambda(s)$ as possible, where $\lambda(0) = 1$ and $\lambda(s)$ has a single dominant pole.

Without this information, implementing this controller would be intuitive guesswork, not that this is itself undesirable, but rather the idea is that if the intuitive approach can be justified with theory, better insight and performance can be obtained.

Thus, it has been shown that the presented method does work under certain conditions and justifies its use in an actual implementation, described in the next chapter. The controller built, while not as complex as that described in this chapter, does work and shows the value of pre-analysis.

# 4. ACTUAL IMPLEMENTATION

## 4.1 Introduction

This chapter describes an implementation of the controller analyzed in the previous chapter. The purpose of the demonstration impedance control system was two-fold: to illustrate the analytical controller and to illustrate the usefulness of impedance control for the performance of certain tasks. Due to computation limitations, the full impedance control version was not built. Instead, the reference model was a simple spring constant, $\underline{K}$, or desired offset from the reference position proportional to measured force: $\underline{f} = \underline{K}(\underline{x}-\underline{r})$.

## 4.2 Hardware and Mechanical Information: The Rhino.

The Rhino XR-1 is a small research oriented robot, produced by Saudu Machine Design Inc. of Champaign, Illinois. It has six degrees of freedom, driven by 12V DC electric motors. Photo 4-1 shows the Rhino. Joint 1 is the elbow, joint 2 the shoulder, joint 3 the waist, joint 4 the wrist, joint 5 the wrist rotation, and joint 6 the gripper. The 2 arm links are both nine inches long.

The control circuit board that comes with the Rhino was not used, as it was too simple for use as is, and would have been too involved to alter. Instead, two interface boards were designed and built by the author. They are shown in Photo 4-2. The board to the rear provided interfacing and motor drive, while the other provided signal conditioning for the load cells

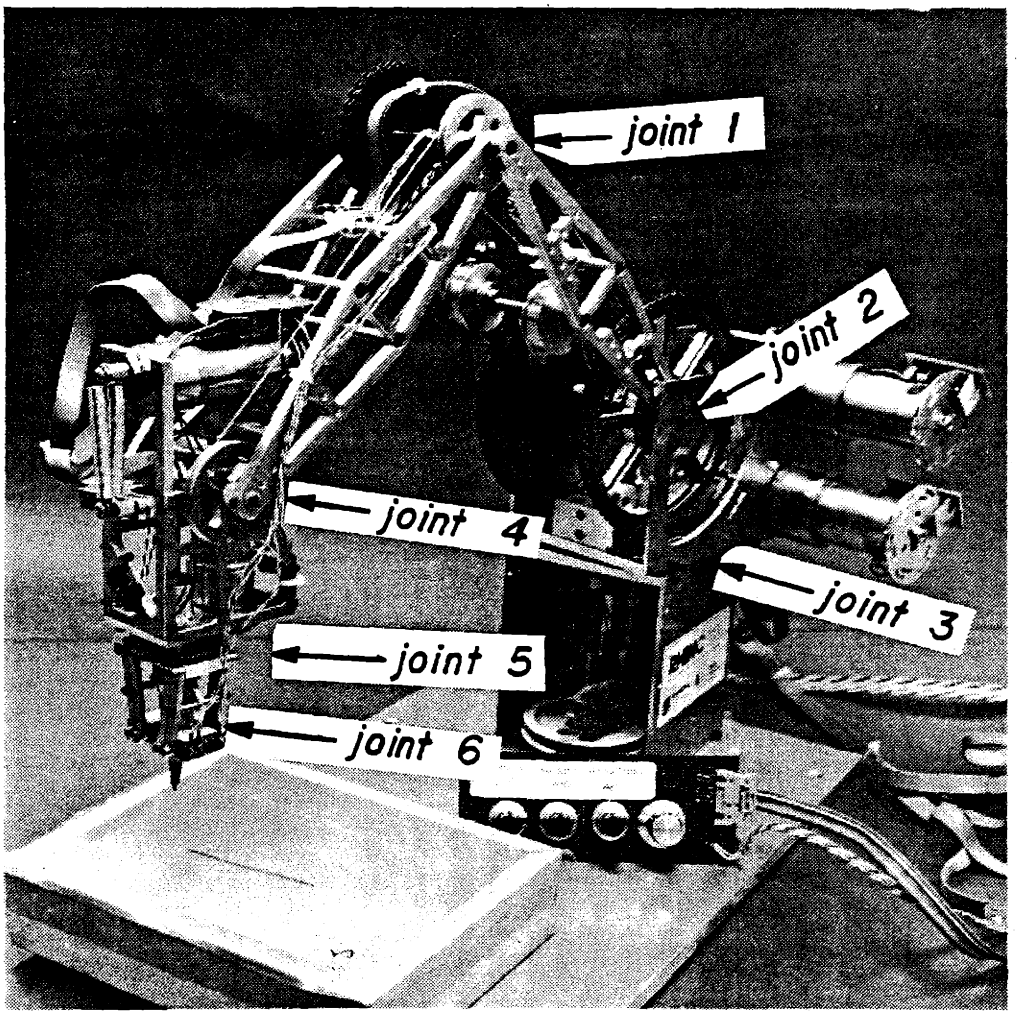


PHOTO 4-1: THE RHINO

(see section 5.3). Both boards are connected to an Intel 8086 mirocomputer system (not shown).. The small control panel on the robot base was used to direct movements. One modification to the robot itself was to replace a rubber belt with a steel chain to prevent slippage and loss of position information.

Fig. 4-1 shows a block diagram of the entire system. An Intel Microcomputer Development System (MDS) was used for software development.

The position decoder takes the position information from the Rhino—in the form of a 2 phase optically generated waveform—and conditions it for the 8086 to interpret. One revolution of the motor (and chopper plate) causes 6 pulses of position information.

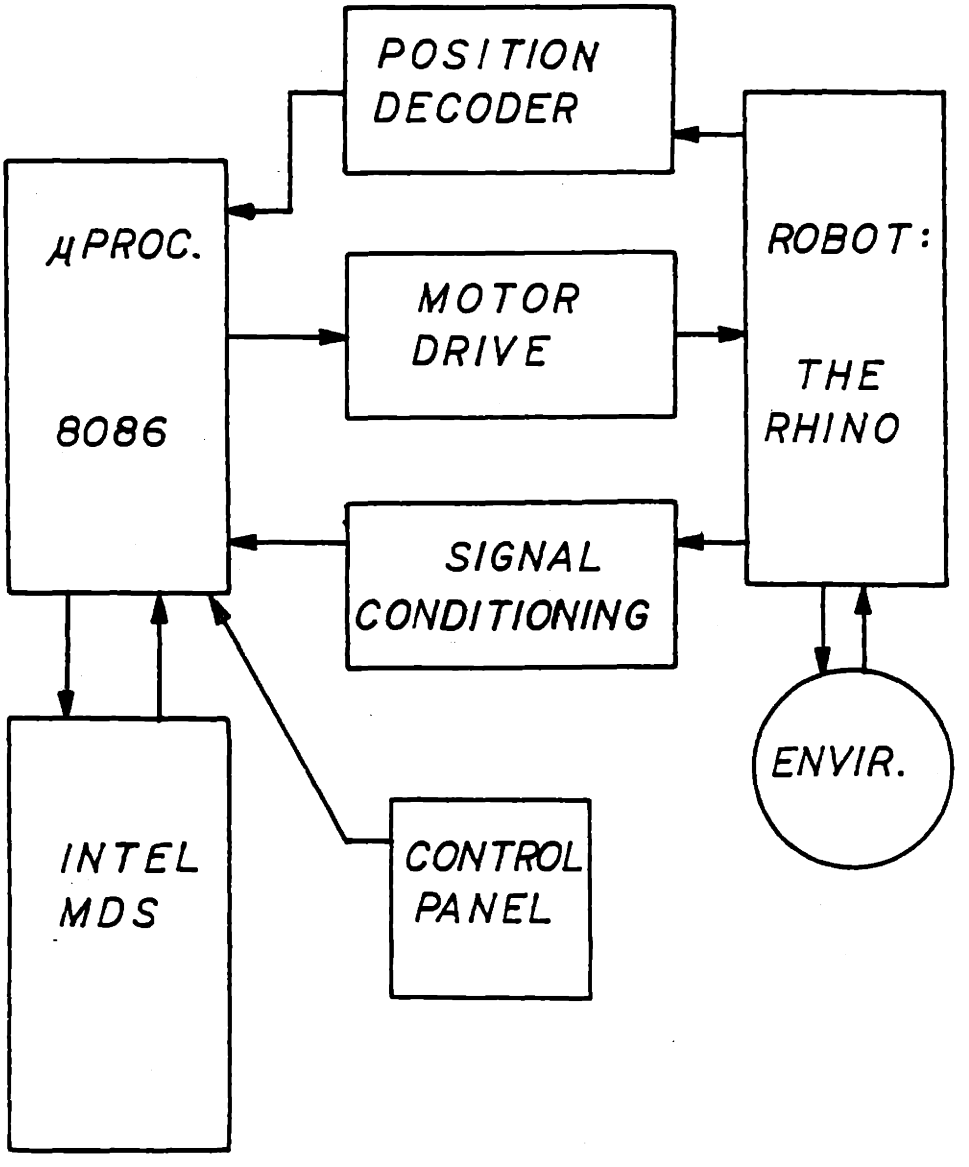


FIGURE 4-1: WHOLE SYSTEM FOR IMPEDANCE CONTROL

## 4.3 Force Sensors

Because load cells to measure small (0-10 oz) forces are scarce, and 3-axis ones even more scarce, it was decided to have custom ones built. They were built by the Materials and Processes Lab of the General Electric Co., Schenectady, New York and are shown in Photos 4-3 and 4-4. They were designed so as to attach directly to the Rhino's gripper (Photo 4-5). Each load cell measures forces in three axes and thus the pair can resolve gripping force as well as x, y, and z forces.

Specifications are:

z axis (vertical) linearity better than 1%
range: 0-500 grams.

x axis (parallel to face) linearity better than 1%
range: 0-500 grams.

y axis (into loadcell) linearity better than 1%
range: 0-2000 grams.

All the axes are very sensitive. With the signal conditioner shown in Photo 4-2 (very inaccurate), forces under 1 gram have been resolved in the z-direction (vertical).

The mounting of the force sensor on the gripper itself is rather unconventional. The usual method is somewhere farther back on the wrist, where it is more isolated from the gripping mechanism. The problem with the gripper mounting is that as an object is squeezed between the jaws, an offset force is set up due to the jaws not being perfectly parallel, or the object not being oriented perfectly. Thus the sensors must be nulled every

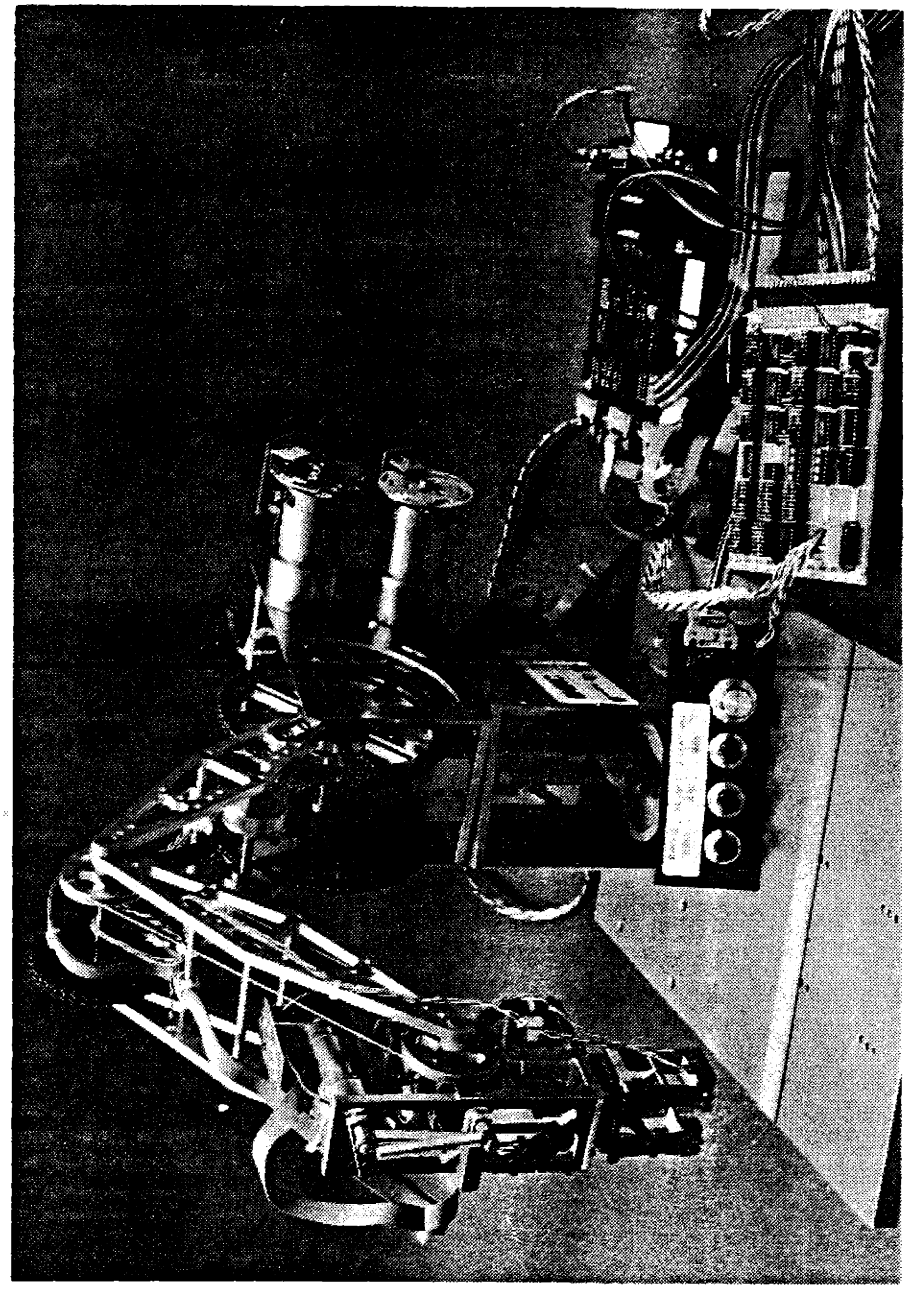

PHOTO 4-2: RHINO WITH INTERFACE HARDWARE

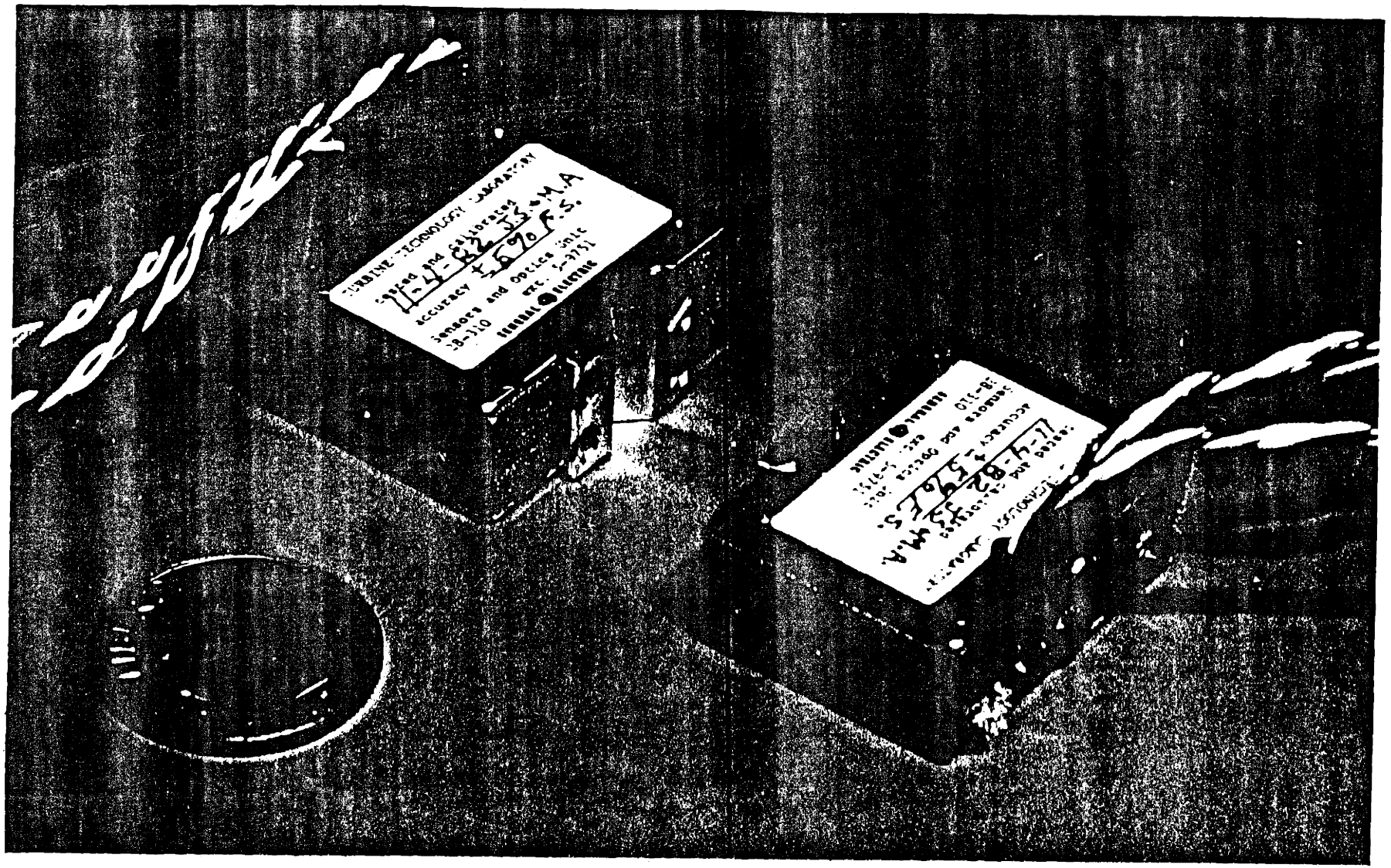

PHOTO 4-3: 3-AXIS LOAD CELLS

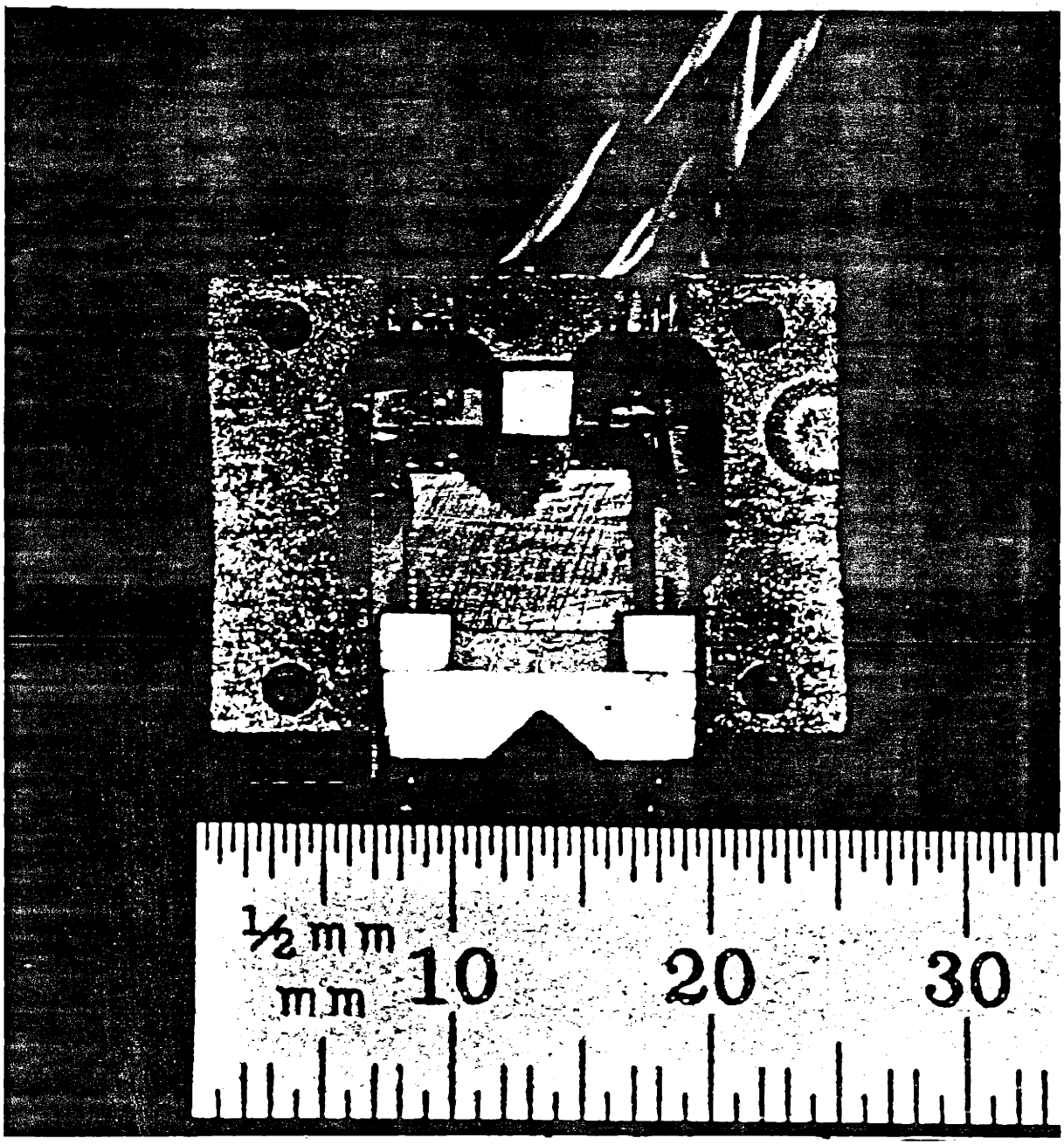


PHOTO 4-4: 3-AXIS LOAD CELL (INTERIOR)

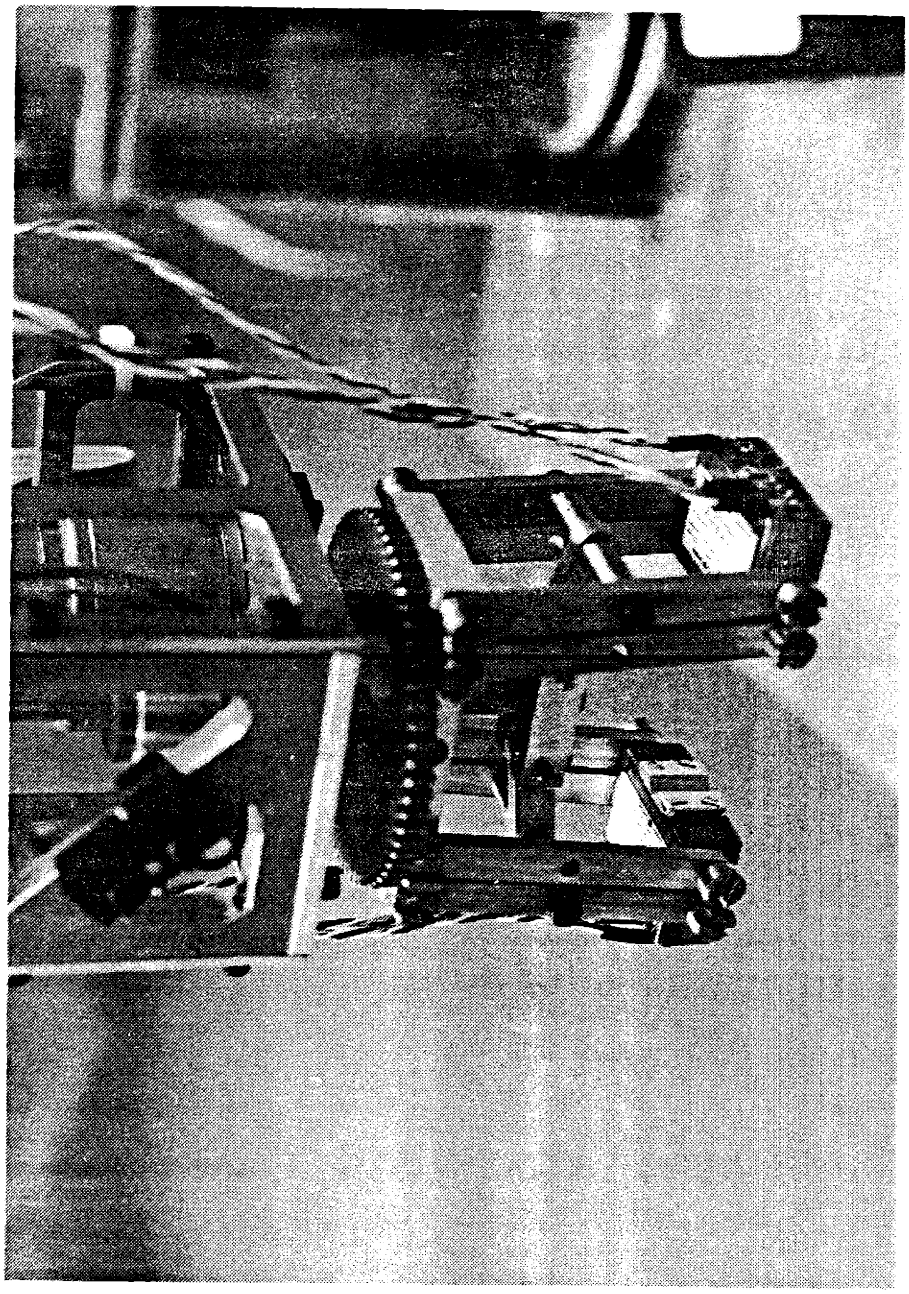

PHOTO 4-5: GRIPPER WITH LOAD CELLS

time an object is picked up. However, this does not greatly interfere with the robot's operation, as the nulling can be performed in software.

## 4.4 Control System Design

If we take the full reference model

$$\underline{M}(s) = [\underline{M}s^2 + \underline{B}s + \underline{K}]^{-1} \qquad (4\text{-}1)$$

and simplify it by making $\underline{M} = 0$ and $\underline{B} = 0$ (or equivalently, only using the DC value), we get

$$\underline{M}(s) = \underline{K}^{-1} \doteq \underline{C} \qquad (4\text{-}2)$$

where C is a compliance (inverse stiffness). Using this in the control scheme of the last chapter, we get the system shown in Fig. 4-2. Note that

$$\underline{e}_x = \underline{K}^{-1}\underline{f} - \underline{x} \qquad (4\text{-}3)$$

implying that $\underline{e}_x = \underline{0}$ causes $\underline{Kx} = \underline{f}$. As before, $\underline{G}(s)$ represents the manipulator dynamics, $\underline{x} = \underline{T}(\underline{\theta})$ is the coordinate transformation, and $\underline{J}$ is the Jacobian of $\underline{T}(\underline{\theta})$. The dotted outline represents the influence of the environment, where $\underline{T}(\underline{\theta})$ has been placed inside this time because this $\underline{T}(\underline{\theta})$ is not computed by the controller, but rather induced by the environment.

The matrix $\underline{P}$ in Fig. 4-2 is a gain in work-space coordinates. It is used to improve performance in directions where the environmental impedance is low. Its use will be explained more fully in section 4.5.

$\underline{K}(s)$ is the tracking regulator's compensator, whose design

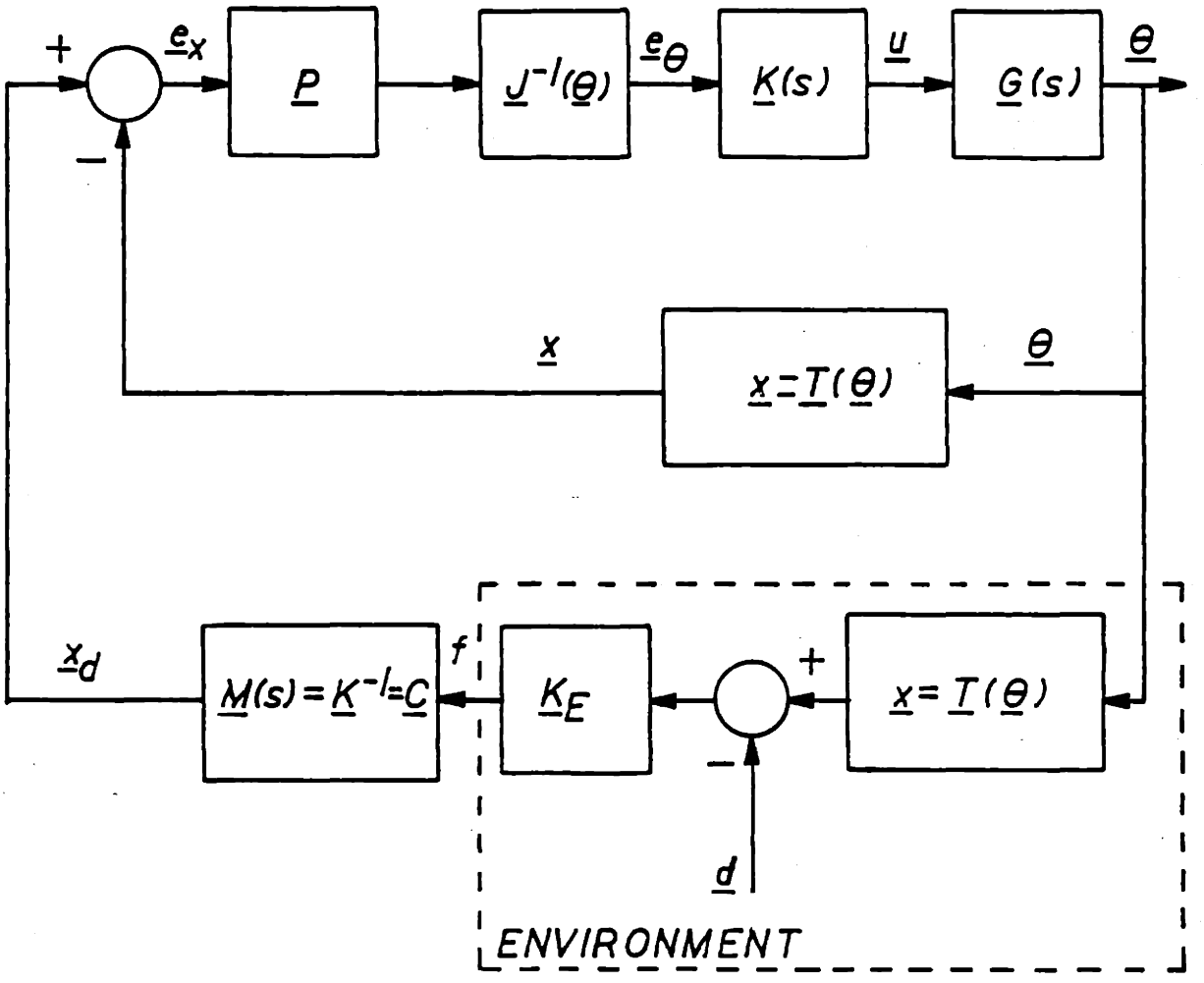


FIGURE 4-2: IMPLEMENTATION OF IMPEDANCE CONTROL FOR THE RHINO XR-1

will be discussed next. Because the Rhino's motors have such a high gear reduction ratio, they appear as virtual velocity controlled servos, and any coupling between joints is insignificant. A mechanical time constant of 0.10 sec was measured and thus a suitable model of typical motor was chosen as

$$g(s) = \frac{1}{s} \cdot \frac{k}{0.1s + 1} \qquad (4\text{-}4)$$

The actual value of k here is unimportant as it depends on where the input signal is defined (motor input, amplifier input, etc.) as well as what the output signal is (rotation in degrees, radiaus, or position encoder holes). Therefore, for this discussion, k = 1 will be assumed.

A block diagram for this motor is shown in Fig. 4-3, where a frictional disturbance has been included. This is important because now $\ddot{\theta}$ can be zero with a non-zero torque, $\tau$, or non-zero input, u, applied. Becauses the disturbance enters before the free integrator, we are not guaranteed zero steady-state error when a position loop is closed around the motor, as shown in Fig. 4-4. Normally, a free integrator is thought of as reducing steady-state errors to zero, but in this case it doesn't. This can be seen by writing the transfer function from $d_f$ to $\theta$ :

$$\frac{\theta(s)}{d_f(s)} = \frac{g(s)}{1 + k(s)g(s)} \qquad (4\text{-}5)$$

where g(s) is the transfer function for the motor. The

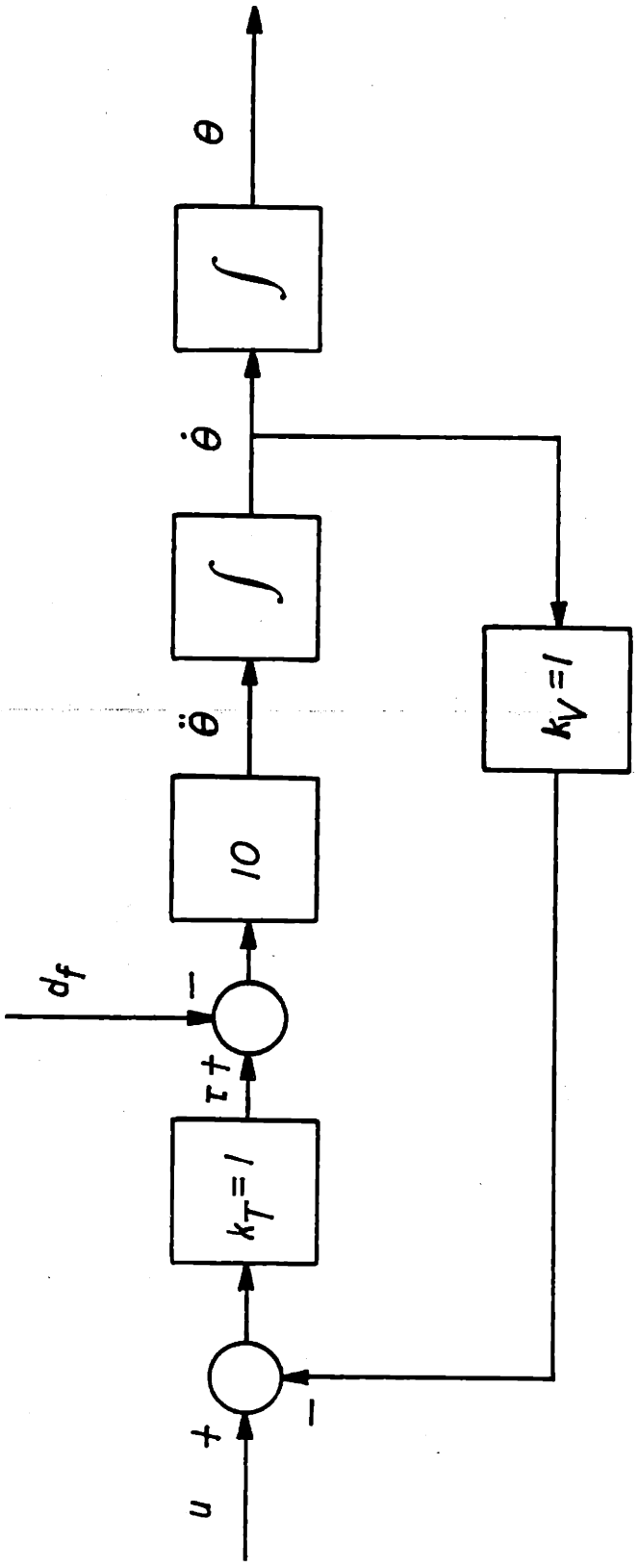


FIGURE 4-3: MOTORS, MANIPULATOR SYSTEM, AND FRICTIONAL DISTURBANCE

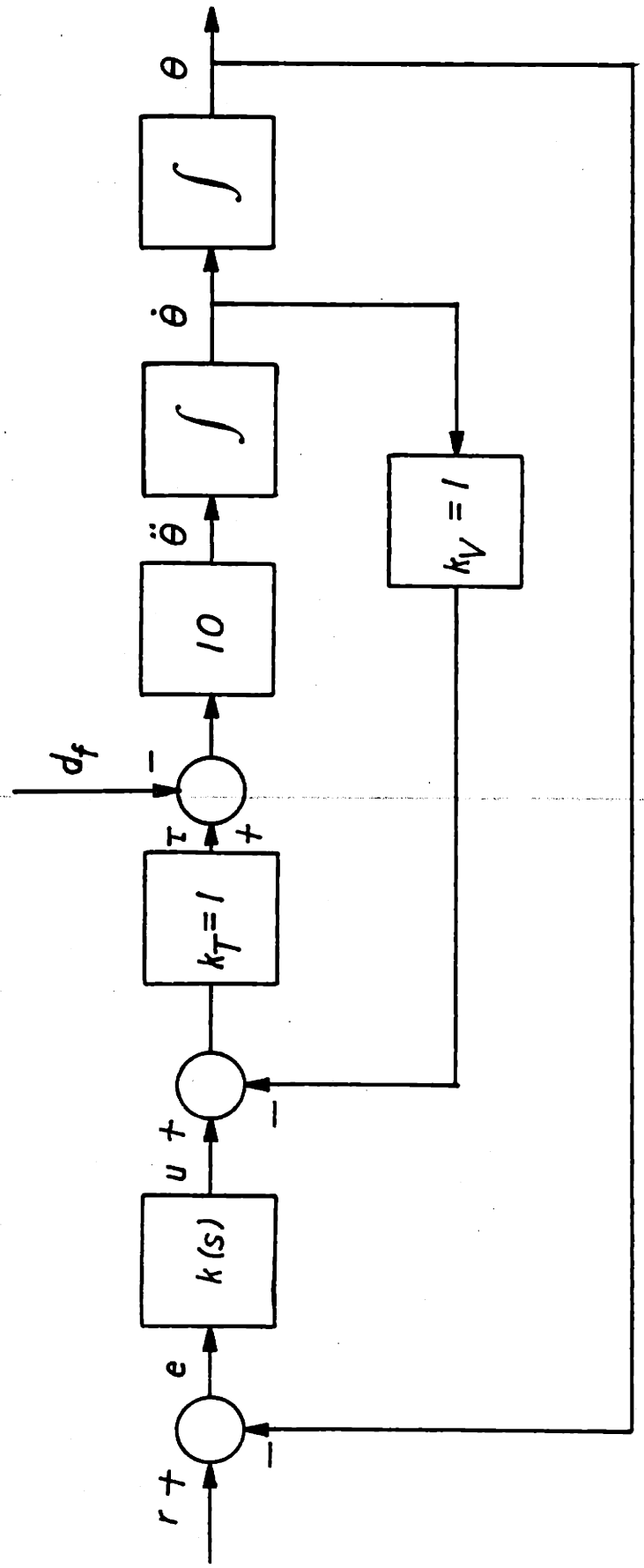


FIGURE 4-4: CLOSED LOOP POSITION CONTROLLER

standard free integrator in k(s) causes $\theta(0)/d_f(0) = 0$, but here we have an integrator in g(s), not k(s). Then $\theta(0)/d_f(0) = 1$ and we don't reject the disturbance. Thus, we will have to provide another integrator in k(s) if we desire zero steady-state errors.

Let us now examine what happens if k(s) = k, a constant. Fig 4-5 shows a root locus as k varies from 0 to $\infty$. As k increases, not only does the bandwidth not increase past 5 rad/sec, but we no longer have one dominant pole. Thus, if we select k(s) = k = 2.0, we get closed-loop poles at approximately -2.8 and -7.2, which are sufficiently separated to provide predominantly one pole roll-off. Notice that if we increase the gain past k = 2, we will increase the bandwidth of $\underline{G}(s)$ and thus $\omega_2$ in Fig. 3-9. While we want a large $\omega_2$, we must have the one-pole rolloff to be able to apply the results concerning reduction of the effect of the coordinate transformation on system stability.

In order to reduce steady-state errors we need to introduce an integrator into k(s)

$$k(s) = k + \frac{P}{s} = \frac{ks + P}{s} \qquad (4\text{-}6)$$

The root locus for k(s)g(s) are shown in Fig 4-6. The zero was placed at -1 (k = P) and a value of k = 4 gives closed-loop poles of -1.45 and -4.28 $\pm$ 3.05j, still dominated by one pole. This k(s) was selected as the final compensator. A bode plot of k(s)g(s) is given in Fig. 4-7. The system has a phase margin of 54°.

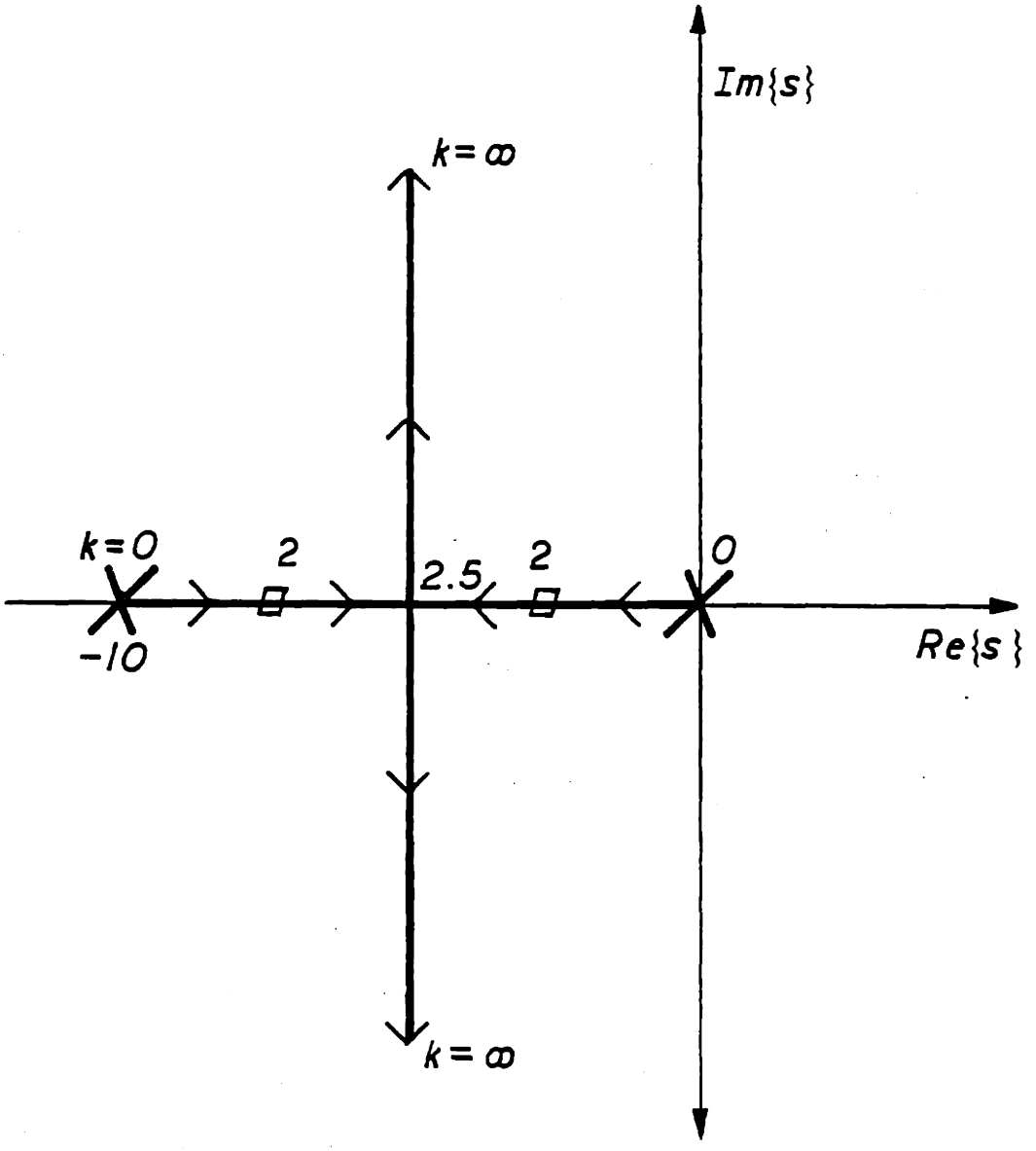


FIGURE 4-5: ROOT LOCUS FOR MOTOR

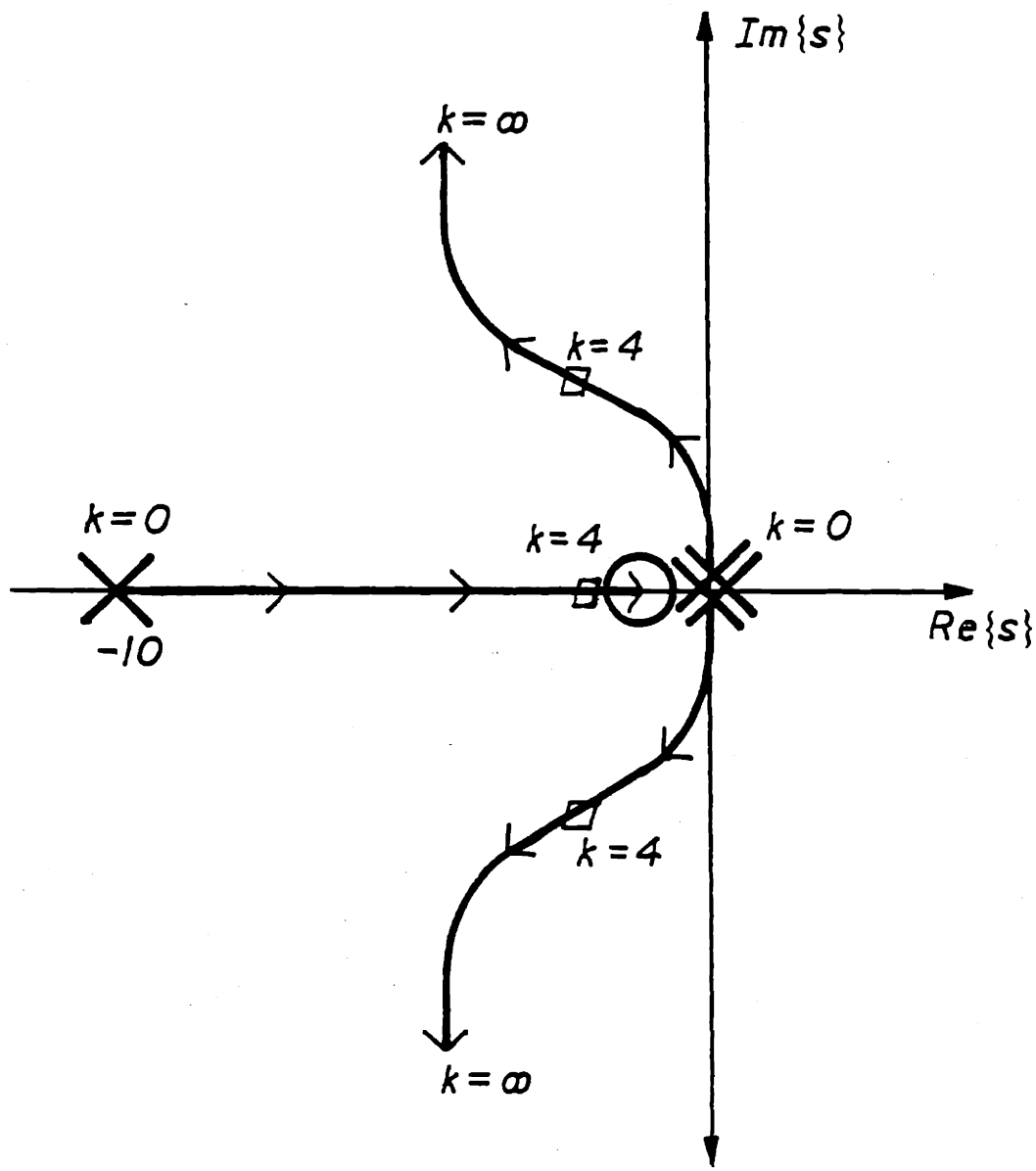


FIGURE 4-6: ROOT LOCUS FOR MOTOR WITH INTEGRAL ACTION

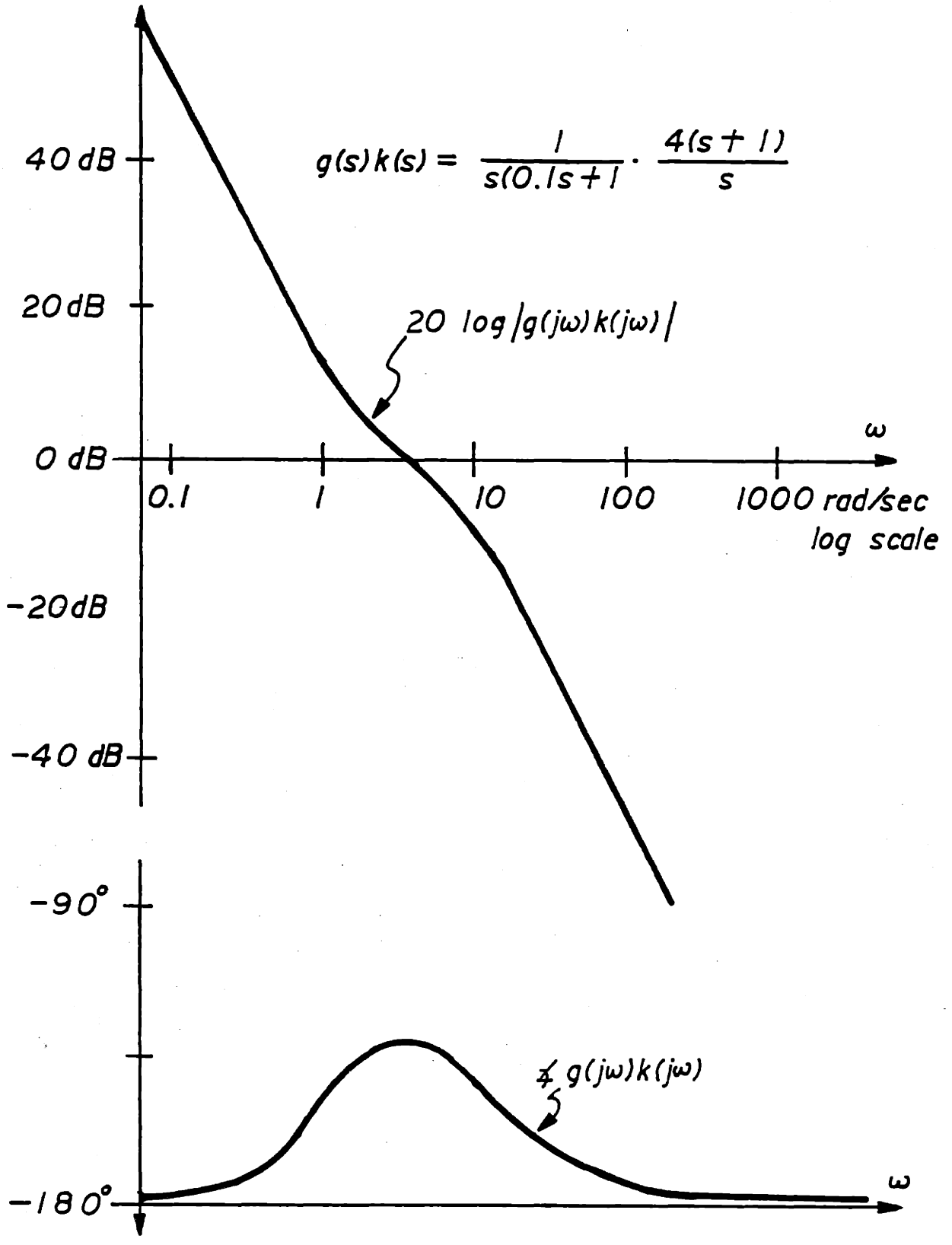


FIGURE 4-7: BODE PLOT OF $g(s)k(s)$

## 4.5 Demonstration

For the demonstration of impedance control the Rhino, only three axes were used: joint 1, 2, and 3 in Photo 4-1. The three smaller knobs shown in that photograph are the reference inputs to the controller: radius, height, and rotation. Thus, the controller works in cylindrical coordinates, rather than cartesian, as too much computation was involved in inverting the 3 x 3 matrix.

All of the computation was done in 16 bit integer arithmetic, which was possible due to proper scaling of variables. Sines and cosines were found by table look-up in a sine table tabulated by degree increments.

A simple top level routine was written which allowed a user to "teach" a series of moves (reference points) to the Rhino, and have them played back, with the impedance control on or off, as desired (off = simple position control). A background procedure ran every 1.0 millisecond and updated the positions of the motors and output the desired voltages via a multiplexed analog line. Fig 4-8 shows an overview of the system software.

As predicted by chapter 3, a stiff surface in the environment could cause instability. This was in fact observed with the Rhino. Fig. 4-9 gives a rough idea of the stability boundary for a particular set of gains. There, $k_Z$ , $k_{EZ}$ represent the desired manipulator stiffness and the environmental stiffness in the z-direction (vertical). This

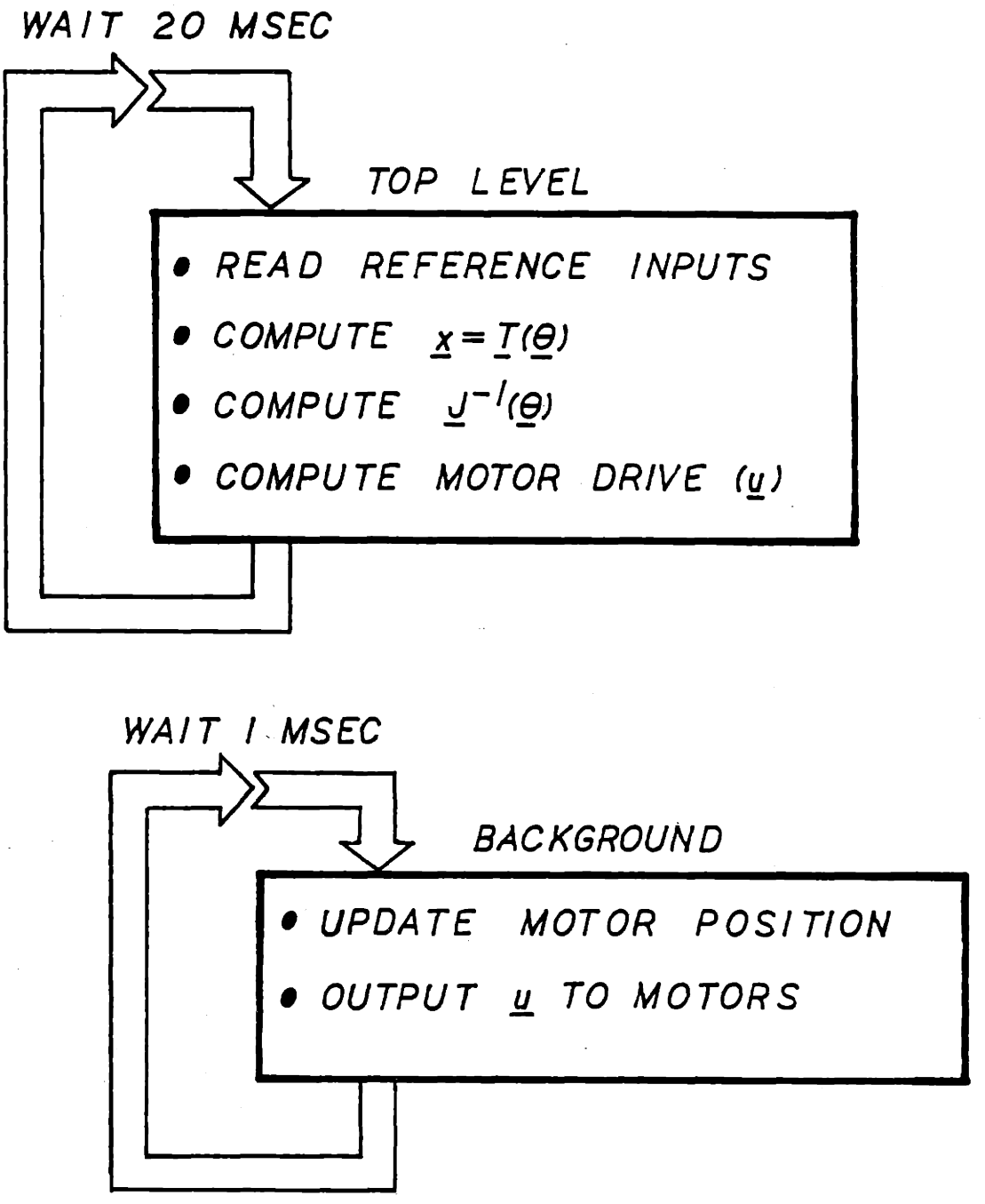


FIGURE 4-8: SYSTEM SOFTWARE

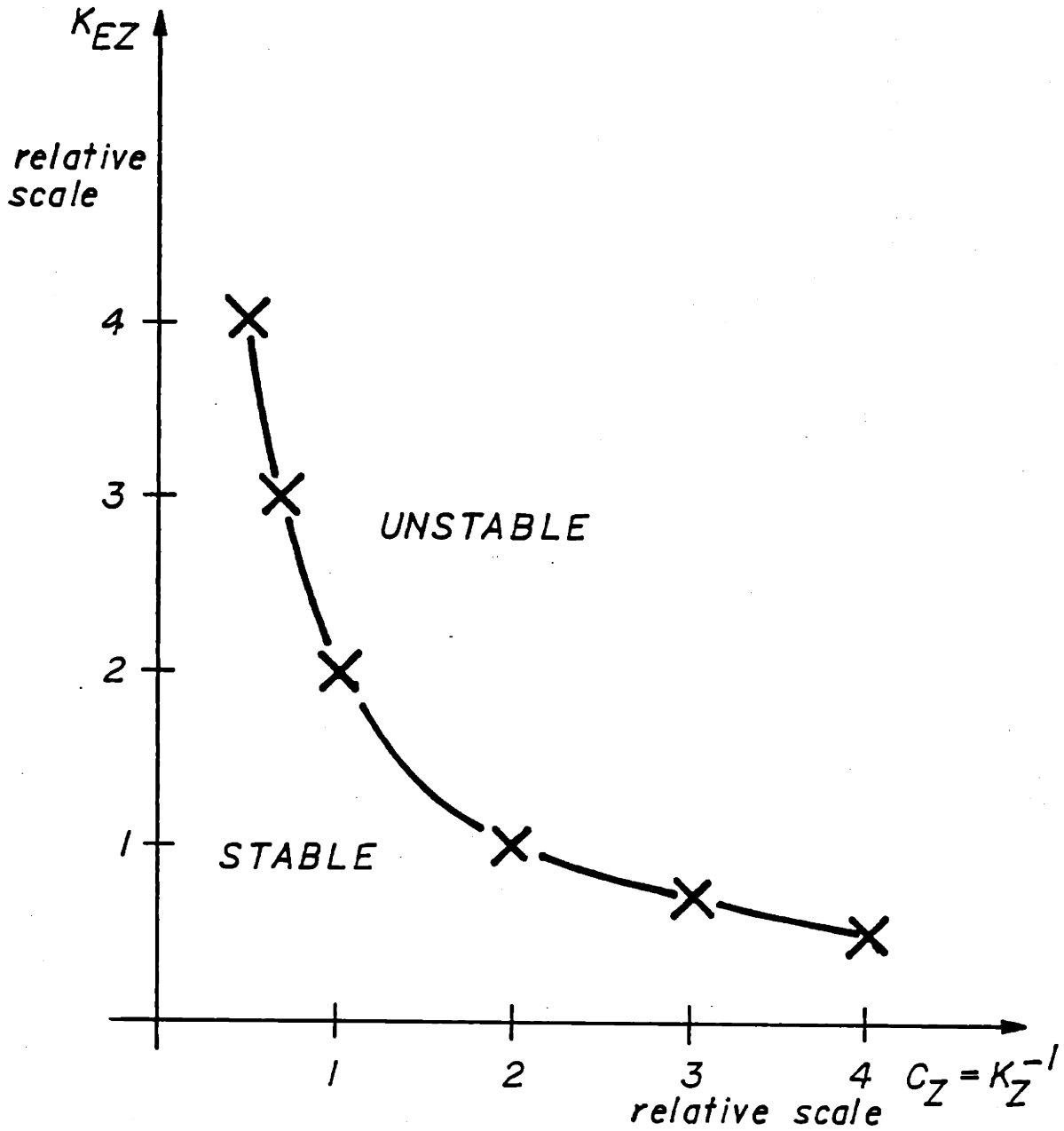


FIGURE 4-9: REGIONS OF STABILITY

graph can be explained by our singular value robustness test.

Since our model is

$$\underline{M}(s) = \underline{K}^{-1} \tag{4-7}$$

and since we are expecting both low speeds and small masses held (a plotter pen in this case), we can assume $\underline{M}_e = 0$, so that

$$\underline{F}(s) = \underline{K}_e \tag{4-8}$$

Under these conditions, our singular value test becomes: system stable if $\sigma_{min}[\ (\underline{K} + \underline{K}_E)\ \underline{K}_E^{-1}\ ] > \sigma_{max}[\underline{J}\underline{H}(s)\underline{J}^{-1} - \underline{I}]$. This is illustrated in Fig. 4-10. Notice that as $\sigma_{max}(\underline{K}_E)$ gets smaller, curve A rises. But as $\sigma_{max}[\underline{K}\ ]$ gets smaller, the curve falls. Thus we can understand the shape of the stability boundary in Fig. 4-9.

Now the presense of the diagonal gain matrix $\underline{P}$ in Fig. 4-2 can be explained. If we make $\underline{P}$ small in a particular channel, we cause curve A in Fig. 4-10 to rise because the curve is really $\sigma_{min}[\underline{I} + (\underline{P}\underline{M}(s)\underline{F}(s)^{-1}\ ]$ when we include $\underline{P}$. The disadvantage of using a very small $\underline{P}$ matrix in all directions is that our performance suffers; $\underline{P}$ is really controlling loop gain and if we make it very small we increase our sensitivity to disturbances.

The reason $\underline{P}$ is included in the controller is that we can selectively raise and lower gains in workspace coordinate channels. For example, suppose we are going to be writing on a hard surface. We simply choose $\underline{P}$ to be "small" in the direction of low stiffness (perpendicular to the surface) and $\underline{P}$ "large" in other directions so as to obtain good performance in controlling

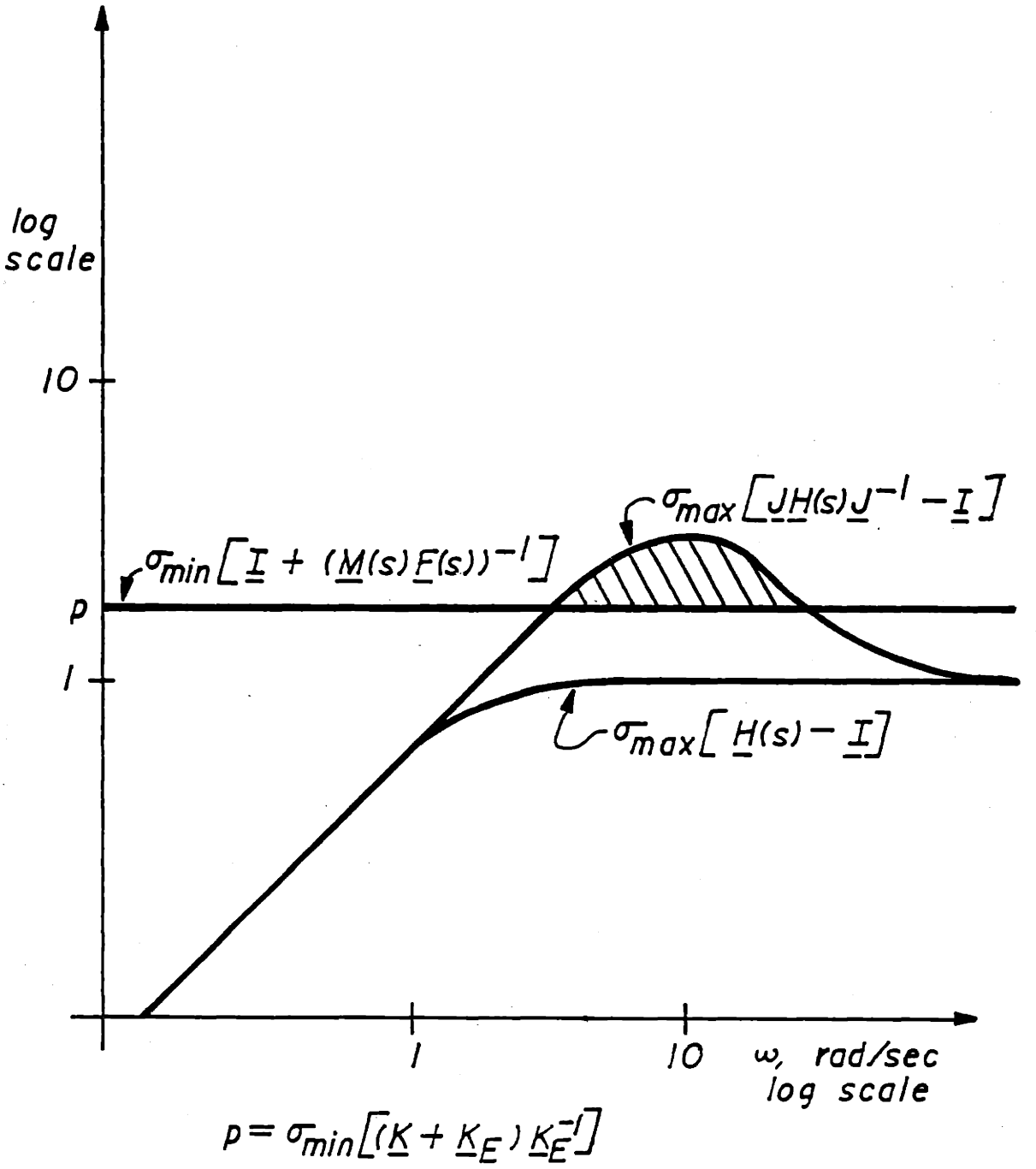


FIGURE 4-10: SINGULAR VALUE ROBUSTNESS TEST

pen movements laterally. Since the controller was designed for $\underline{P} = \underline{I}$, choosing $\underline{P}$ "small" means increasing the gain for good performance (to 2, say, seen from root locus).

The robot/controller system was used in a variety of demonstrations. Some of the more interesting ones will be described here. Also, a videotape presentation was prepared showing the robot in operation writing on thin sheets of paper held in a frame.

One demonstration involved writing with uncertainty. With a pen held in the gripper, the robot was programmed to write on a pad of paper on the table. In between repetitions, a one-half inch pad was slipped under the paper. The robot still managed to write on the surface. With a standard (stiff) manipulator, the pen would have been destroyed by such a maneuver.

Another demonstration involved writing on a sheet of paper held tightly in a space frame. Photo 4-1 shows the frame with a sheet of plastic. The robot could write on the paper, with impedance control turned on (compliant), even as the frame was moved vertically or tilted horizontally. For these demonstrations, the compliance was set low in the horizontal directions and high vertically. This allowed the robot to track reference positions accurately horizontally but be compliant vertically to allow for uncertainty.

## 4.7 Conclusion

This chapter has briefly described an implementation of an impedance controller for a robotic manipulator. The robot was capable of performing certain tasks under uncertainty that would have been exceedingly difficult without impedance control or extra external sensors. It also served as a simple demonstration of some of the analytical results of the last chapter. Due to limitations on computational ability and to the simplicity of the Rhino (high-gear reduction DC motors), a complex controller was not used. However, the main point of the demonstration was to provide some insight into the types of tasks amenable to impedance control and the capabilities of such a system.

# 5. CONCLUSION

## 5.1 Summary

This thesis has attempted to show the benefits of a class of force control for robotics and present some basic information on its implementation.

Impedance control, one type of force control, has many benefits, such as the ability to perform certain classes of tasks under uncertain or changing conditions. By mimicking the techniques humans use in performing tasks, a robot can be equipped to handle writing, sanding, and scraping on surfaces with uncertain position. Cranks can be turned and doors opened without exact knowledge of their parameters.

In order to demonstrate these concepts first an analytical robustness verification of the viability of a linear controller of assumed form was presented in chapter three. This verification thus allowed the implementation to proceed: some hardware was designed and built, load-cells were custom built, and approximately 2k of 8086 assembly code was written. Some of these details were presented in chapter 4. The actual impedance control equipped robot was then used to demonstrate the capability of force control. A video tape presentation of approximately five minutes duration was then made to provide illustration of these principles.

## 5.2 Suggestion for Future Research

Obviously, many questions are still unanswered in terms of implementing impedance control. Some of them are as follows.

Is there any way of further reducing the conservativeness of the robustness test presented in chapter 3? Perhaps a new test would be better.

If this linear controller cannot be improved, is there a better form for the controller? Due to the large parameter variations of the environment and possibly the manipulator, perhaps a linear control method will not suffice—adaptive control is one possibility.

Aside from the implementation issue, there are questions about choosing the actual model reference parameters--i.e. the stiffness, damping, and mass of the reference. Does it matter what the exact values of these parameters are? If it is important, how should they be chosen?

## REFERENCES

[1] Andrews, R.J., Douli Systems: Design and Construction and Controller for Research in Impedance Control, S.B. Thesis, Dept. of Mech. Engineering, M.I.T., June 1981.

[2] Hewit, J.R. and Burdess, J.S., "Fast Dynamic Decoupled Control for Robotics, Using Active Force Control," Mechanism and Machine Theory, Vol. 16, 1981.

[3] Hewit, J.R., and Padovan, J., "Decoupled Feedback Control of Robot and Manipulator Arms," 3rd Symposium: Theory and Practice of Robots and Manipulators CISM - IFTOMM Italy, September 1978.

[4] Hogan, N., and Cotter, S.L., "Programming Cartesian Impedance on a Nonlinear Manipulator," 1982 ASME WAM Robotics Symposium, 1982.

[5] Lehtomaki, N., Practical Robustness Measures in Multivariable Control System Analysis, M.I.T. Laboratory for Information and Decision Systems, Ph.D. Thesis, LIDS-TH-1093, 1982.

[6] Mason, Mathew T., "Compliance and Force Control for Computer Controlled Manipulators," IEEE Transactions on Systems, Man, Cybernetics, Vol. SMC-11, No.6, June 1981.

[7] Paul, Richard P., Robot Manipulators. M.I.T. Press, 1981.

[8] Salisbury, J. Kenneth, "Active Stiffness Control of a Manipulator in Cartesian Coordinates," Proc. of IEEE Conference on Decision and Control, 1980.

[9] Tyler, J.S., Jr., "The Characteristics of Model-Following Systems as Synthesized by Optimal Control," IEEE Transactions or Automatic Control, Vol. AC-9, No. 4, Oct. 1964, pp. 485-498.

[10] Whitney, Daniel E., "Force Feedback Control of Manipulator Fine Motions," ASME Journal Dynamic Systems Measurement and Control, June 1977.